Article

Not peer-reviewed version

Ferrocene-Catalyzed Aromatization and Competitive Oxidative Ring Transformations of 1,2,4a,8a-tetrahydro-1-arylpyridazino[4,5-d]pyridazines

Dániel Hutai , Tibor Zs. Nagy , Veronika Emődi , Antal Csámpai *

Posted Date: 16 June 2025

doi: 10.20944/preprints202506.1204.v1

Keywords: pyridazino[4,5-d]pyridazine; DDQ-mediated dehydrogenative aromatization; ferrocene-catalyst; SET; DFT-supported reaction mechanism; oxidative dimerization; aryne-generating fragmentation; Diels-Alder-retro Diels-Alder sequence; NMR structural elucidation.

 doi:10.20944/preprints202506.1204.v1

Article

Ferrocene-Catalyzed Aromatization and Competitive Oxidative Ring Transformations of 1,2,4a,8a-tetrahydro-1-arylpyridazino-[4,5-d]pyridazines

Dániel Hutai, Tibor Zs. Nagy, Veronika Emődi and Antal Csámpai *

Department of Organic Chemistry, Chemistry, Eötvös Loránd University (ELTE), Budapest, H-1117 Budapest, Hungary

* Correspondence: antal.csampai@ttk.elte.hu; Tel.: +36-13722500/6591

Abstract: This paper presents the expected and unexpected, but typically substituent-dependent ferrocene-catalysed DDQ-mediated oxidative transformations of a series of 5,8-*bis*(methylthio)-1-aryl-1,2-dihydropyridazino[4,5-*d*]pyridazines (**1a–e**) and 8-(3,5-dimethyl-1*H*-pyrazol-1-yl)-5-(methylthio)-1-aryl-1,2-dihydropyridazino[4,5-*d*]pyridazines (**2a–e**). Under noncatalytic conditions the reactions of **1a–e** were sluggish producing substantial amount of undefined tarry materials, but the reactions catalysed by ferrocene gave the aromatic products **3a–e** in markedly higher isolated yields. The expected aromatizations were accompanied by ring-transformations proceeding *via* aryne-generating fragmentation/Diels-Alder (DA)/N_2-releasing retro Diels-Alder (rDA) sequence to construct arene-fused phthalazines type **5**. On the other hand, neither the noncatalytic nor the catalytic reactions of **2a–e** yielded the expected aromatic products. Instead, depending on their substitution pattern, the catalytic reactions of these pyrazolyl-substituted precursors also led to the formation of dearylated arene-fused phthalazines type **6** competing with unprecedented multistep fragmentation sequence terminated by the hydrolysis of cationic intermediates type **30** to give 4-(methylthio)pyridazino[4,5-*d*]pyridazin-1(2*H*)-one (**7**) and the corresponding 3,5-dimethyl-1-aryl-1*H*-pyrazole type **8**. When 0.6 equivalent of DDQ was applied in freshly absolutized THF, the 2-naphthyl derivative **2c** underwent an oxidative coupling to give dimer **32c** formed by the interaction of cationic intermediate **30c** and the *N*-nucleophilic precursor remained intact. In a cross-experiment with a 1:1 mixture of **2c** and **1c** the formation of the dimer **34c** substituted with three methylthio groups refers to the coupling of cation **30c** and the intact **1c** which proved to be more resistant to oxidation compared to the cation-generating **2c**. Under the same conditions besides **32c** and **34c**, 1-butoxy-4-(methylthio)- pyridazino[4,5-*d*]pyridazine **33** was also formed in a sequential nucleophilic displacement-transfer hydrogenation process with the involvement of cation **30c** and two solvent molecules probably serving as a nucleophile and a reductive agent. A systematic computational study was conducted on the intriguing reactions to support their complex mechanisms proposed on the basis of the structures of the isolated products.

Keywords: pyridazino[4,5-*d*]pyridazine; DDQ-mediated dehydrogenative aromatization; ferrocene-catalyst; SET; DFT-supported reaction mechanism; oxidative dimerization; aryne-generating fragmentation; Diels-Alder-retro Diels-Alder sequence; NMR structural elucidation

1. Introduction

Representing privileged scaffolds among therapeutically active small molecules structurally diverse pyridazines and their condensed analoges continue to attract considerable interest in pharmaceutical chemistry. Besides the bioactive pyridazine-based compounds found among anti-HIV [1], antiviral [2], antibacterial [3], antihypertensive [4], and anti-inflammatory [5] agents, pyridazine derivatives have also been identified as highly potent anti-cancer drug candidates [6–10].

 doi:10.20944/preprints202506.1204.v1

On the other hand, much less attention has been paid to pyridazino[4,5-d]pyridazine ring system. Only a limited number of its 1,4-disubstituted derivatives are known in the literature [11–17].

The introduction of different substituents into positions 5 and 8 seems to be a crucial point in the extension of the group of this class of heterocycles. In one of our previous papers we described the regioselective synthesis of a few 1,2,4a,8a-tetrahydro-1-arylpyridazino[4,5-d]pyridazines **1a**-**e** and **2a**-**e** (Scheme 1) achieved by substituent-directed addition of polar organometallic reagents on the 1,4-*bis*-methylthio-and 1-(3,5-dimethyl-1*H*-pyrazol-1-yl)-4-methylthio derivatives **I** and **II**, respectively, used as easily available precursors [18]. As an extension of our research focusing on the synthesis, functionalization of pyridazines including condensed analogues with potential and proved antiproliferative activity [19–23], we envisaged the dehydrogenation of the aryl adducts **1a**-**e** and **2a**-**e** to access **3a**-**e** and **4a**-**e**, respectively, the aromatic products (Scheme 1) for antiproliferative assays aimed at the extension of SAR established for related heterocycles with fused pyridazine moiety [6–10,20–22]. On the other hand, the targeted bicyclic heteroaromatics can be considered as diazadiene components in inverse-electron demand Diels-Alder (DA) reactions followed by N_2-eliminating retro-DA process (rDA) constructing phthalazines with versatile substituent patterns [13].

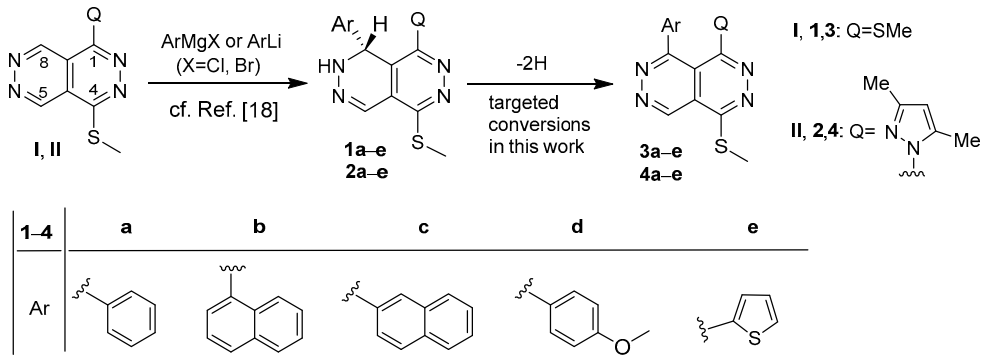

Scheme 1. Envisaged dehydrogenative aromatization reactions converting addition-derived 5,8-*bis*(methylthio)- and (3,5-dimethyl-1*H*-pyrazol-1-yl)-5-(methylthio)-1-aryl-1,2-dihydropyrid- azino[4,5-d]pyridazines **1a–e** and **2a–e** into the corresponding aromatic products **3a–e** and **4a–e**, respectively.

A large variety of non-catalytic and catalytic oxidative dehydrogenative aromatization methods have been elaborated for the oxidative dehydrogenation of saturated or partly saturated ring systems to diversely functionalized aromatic scaffolds of potential biological interest including pyrroles, pyrazoles, imidazoles, oxazoles, thiazoles, quinolones, isoquinolines, pyridines, pyrimidines, triazines, pyridazines and β-carbolines as revied extensively [24,25]. Most of the reported conventional protocols are based on the use of MnO_2 [26,27], o-iodoxybenzoic acid (IBX), [28–30], NBS [31,32], NCS [33] di-tert-butyl peroxide (DTBP) [34], $Pb(OAc)_4$ [35], $PhI(OAc)_2$ [36], $PhI(OTFA)_2$ [37], S_8 [37,38], trichloroisocyanuric acid (TCCA) [39], I_2 [40], benzoyl peroxide (BPO) [41], ceric ammonium nitrate (CAN) [42], chromium(VI) reagents [43], selenium dioxide [44] and DDQ [45–51] as stoichiometric reagents. Catalytic methods have also been elaborated exploring iodine [52,53] and a plethora of metal-based systems nanoparticles, metal-organic frameworks, photoredox-activated complexes and enzymes as catalysts, most of them combined with molecular oxygen as a terminal oxidant or used under the conditions of acceptorless dehydrogenation [54–74]. However, due to the involvement of highly specialized catalytic systems and experimental set-up these dehydrogenation protocols are often expensive and cannot be considered as scale-up strategies for the batch synthesis of the targeted compounds. On the other hand, DDQ has been identified as one of the most widely applicable stoichiometric and and easy-to-handle oxidant in dehydrogenative aromatization of *N*-heterocycles. In the context of our synthetic goals it is of pronounced importance that partially saturated pyridazines such as in situ generated 1,6-dihydropyridazines were also readily converted into pyridazines via oxidative aromatization by DDQ [50,51]. Accordingly, we first attempted to use

 doi:10.20944/preprints202506.1204.v1

this oxidant for converting **1a–e** and **2a–e** into aromatic pyridazino[4,5-*d*]pyridazines **3a–e** and **4a–e**, respectively (Scheme 1).

2. Results

In the first set of experiments, we attempted to perform simple non-catalytic DDQ-mediated aromatization of the *bis*-methylthio derivatives **1a–e**. The reactions conducted for 5 h in the presence of DDQ (1.2 equiv.) in polar solvents (MeCN, THF and DMSO) at 60 °C (Methods A–C: Scheme 2) allowed the isolation of the expected products **3a–e** only in low yields (14–24%: Table 1). The TLC analysis of the reaction mixtures showed a significant reluctance of **1a–e** to undergo any appreciable transformation below this temperature. However, under the conditions of Methods A–C the dehydroaromatisation reactions leading to **3a–e** were accompanied by the formation of substantial amounts of decomposition products preventing the recovery even of a small portion of the precursors. Under the same non-catalytic conditions, the attempted dehydrogenations of **2a**,**b**,**d**,**e** gave no identifiable products as these pyrazolyl-substituted precursors underwent practically complete decomposition. On the other hand, an angularly condensed naphtho-fused phthalazine (**6c**: Scheme 2) could be isolated in low yields (7–12%) from the mixtures obtained by the reactions of 2-naphthyl analogue **2c** (Table 1). Since the aforementioned noncatalytic reactions proved to be unsatisfactory from the point of view of our synthetic purposes, we attempted to perform the dehydroaromatisations of **1a–e** and **2a–e** in the presence of a catalytic amount (5%) of ferrocene expected to act as redox catalyst [75–81] capable of undergoing fast and kinetically uncomplicated reversible redox change by single electron transfer (SET) which might be beneficial in terms of activating mechanistic pathways leading to the targeted bicyclic aromatic products **3a–e** and **4a–e** with enhanced selectivity. Accordingly, with the intention of improving the synthetic outcome of the synthetic experiments circumventing uncontrolled transformations, the reactions of **1a–e** were performed under the conditions of Methods D–F using shortened reaction time (3 h) to circumvent or suppress further undesired transformations of the products into tarry materials. The reactions run at 60 °C afforded not only **3a–e**, but also fused phthalazines (**5a** and **5bc**) along with **I** derived from a specific dearylation process, as interpreted in detail in the next session. The progress of the reactions was monitored by TLC which indicated again a definite slowdown of the detectable transformations of the substrates below 60 °C. All products were isolated in low-to-mediocre yields (Scheme 2, Table 1). Due to molecular symmetry both 1-naphthyl- and 2-naphthyl-substituted precursors **1b** and **1c** gave identical angularly condensed naphtho[2,1-*g*]phthalazine (**5bc**) in yields comparable to those achieved in the isolation of the appropriate aromatic products type **3**. It must be pointed out that under the same conditions 4-methoxyphenyl derivative **1d** got converted into **3d** as the exclusively isolable product in acceptable-to-good yields (68–80%: Table 1).

Table 1. Methods and product distributions of the DDQ-mediated oxidative transformations of 5,8-bis(methylthio)-1-aryl-1,2- dihydropyridazino[4,5-*d*]pyridazines **1a–e** and 8-(3,5-dimethyl-1*H*-pyrazol-1-yl)-5-(methylthio)- 1-aryl-1,2-dihydropyridazino[4,5-*d*]pyridazines **2a–e**.

entry	precursor	product(s).	Yields by A (%/%)	Yields by B (%/%)	Yields by C (%/%)	Yields by D (%/%)	Yields by E (%/%)	Yields by F (%/%)
1	**1a**	**3a/5a/Ia**	14/–/–	16/–/–	18/–/–	37/24/5	45/22/6	43/30/6
2	**1b**	**3b/5bc/I**	17/–/–	21/–/–	19/–/–	35/34/7	41/35/6	39/32/7
3	**1c**	**3c/5bc/I**	16/–/–	16/–/–	19/–/–	31/24/5	37/34/11	32/40/8
4	**1d**	**3d**	17	20	24	74	68	80
5	**1e**	**3e/I**	17/–	20/–	22/	59/18	47/20	64/24
6	**2a**	**6a/II/7/8a**	–/–/–/–	–/–/–/–	–/–/–/–	19/20/7/23	26/13/9/19	30/19/8/24
7	**2b**	**6c/II/7/8a**	–/–/–/–	–/–/–/–	–/–/–/–	20/10/17/12	20/8/24/18	26/9/32/25
8	**2c**	**6c/II/7/8a**	8/–/–/–	12/–/–/–	7/–/–/–	25/8/36/21	22/10/41/27	25/9/43/32
9	**2d**	**7/8d**	–/–	–/–	–/–	44/37	37/44	46/49
10	**2e**	**II**	–	–	–	52	59	64

 doi:10.20944/preprints202506.1204.v1

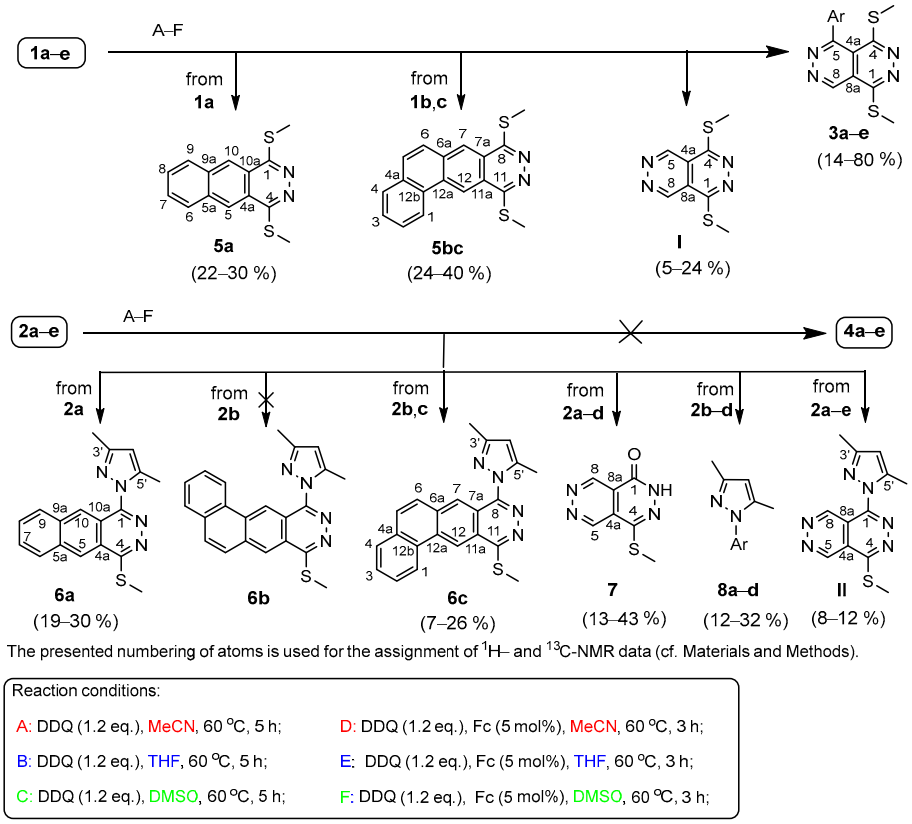

The presented numbering of atoms is used for the assignment of ^{1}H– and ^{13}C-NMR data (cf. Materials and Methods).

Reaction conditions:

A: DDQ (1.2 eq.), MeCN, 60 °C, 5 h; D: DDQ (1.2 eq.), Fc (5 mol%), MeCN, 60 °C, 3 h;

B: DDQ (1.2 eq.), THF, 60 °C, 5 h; E: DDQ (1.2 eq.), Fc (5 mol%), THF, 60 °C, 3 h;

C: DDQ (1.2 eq.), DMSO, 60 °C, 5 h; F: DDQ (1.2 eq.), Fc (5 mol%), DMSO, 60 °C, 3 h;

Scheme 2. Non-catalytic and catalytic aromatization reactions of the 1-aryl-1,2-dihydropyridazino[4,5-*d*]pyridazines and competitive oxidative ring transformations.

Irrespective of the nature of the aryl group bonded to C1 position, the reactions of **2a–e** carried out by Methods D–F did not provide the expected bicyclic heteroaromatics **4a–e**. Instead, besides fused phthalazines **6a**,**c**, two dearylated pyridazino[4,5-*d*]pyridazine derivatives **7** and **II** along with *N*-arypyrazoles type **8a–d** could be isolated from the reaction mixtures in low-to-mediocre yields (Scheme 2 and Table 1).

It was an intriguing experience that both **2b** and its isomer **2c** got converted into identical angular naphtho-fused pyrazolyl-phthalazine (**6c**) of which isomer **6b** could not be isolated from the mixtures obtained by the reactions of **2b**. While phthalazines were formed only in the reactions of **2a–c**, under the applied conditions each member of the investigated group of precursor type **2** gave dearylated product **7.** It must be pointed out here that the definite complementarity clearly reflected from the structures of **7** and the isolated *N*-arylpyrazoles **8a–d** suggests that these products are generated *via* connected fragmentation pathways associated with intramolecular *N*-arylation and hydrolytic fission of the pyrazolyl substituent on the pyridazino[4,5-*d*]pyridazine scaffold as will also be discussed in the next session. On the other hand, we also observed another intriguing difference in the outcomes of the experiments performed with **2d** and **2e**. While the reactions of **2d** performed by Methods D-F afforded only **7** and **8d** in mediocre, but comparable yields, the reactions of thienyl-substituted precursor **2e** gave dearylated aromatic heterocycle **II** as exclusively isolable product (Table 1).

3. Discussion

Apart from the realization of the expected dehydroaromatisations **1a–e** → **3a–e**, the intriguing outcome of our synthetic experiments obviously needs to be rationalized by such mechanistic pathways that can provide reasonable rationale for the formation of a number of unexpected products. However, first it is necessary to declare that besides **1a–e** → **3a–e** the analogous dehydroaromatizations **2a–e** → **4a–e** are also feasible from the point of view of their thermodynamics

 doi:10.20944/preprints202506.1204.v1

reflected from the change in free energy associated with these transformations almost invariant to the substituents of the bicyclic heteroaromatic framework (ΔG in [kcal/mol] for the overall reactions **1** + DDQ → **3** + $DDQH_2$: **a** –33.6; **b** –33.2; **c** –33.3; **d** –36.6; **e** –34.5. / ΔG in [kcal/mol] for the overall reactions **2** + DDQ → **4** + $DDQH_2$: **a** –32.9; **b** –32.2; **c** –33.8; **d** –34.8; **4** –33.9). Thus, it was necessary to generate mechanistic pathways comprising such specific elementary steps that suitable to account for the intriguing formation of the unexpected products isolated and identified in our experiments (Scheme 3). Since the catalytic reactions of **1a–c** and **2a–c** allowed the isolation of all types of products first we focused on the transformations of these precursors to support our view about the complex mechanisms (Scheme 3).

In order to reveal the feasibility of the competing pathways assumed to construct the different structures, we performed a series of comparative DFT modelling studies on the most relevant elementary steps expected to be involved in branched pathways (Scheme 3). In the course of the DFT calculations, the optimisation and subsequent frequency calculation on molecular structures were carried out with M06-2X global functional [82] using 6-31 G(d,p) basis set [83] supplemented by IEFPCM solvent model [84]. For these computations dielectric constant was set to 47 to represent the polarity of DMSO used as solvent by Method F that – in most cases -provided the highest yields of the isolable products.

Prior to analysis of the pathways assumed to be operative in the ferrocene-catalyzed conversions, we calculated the energetics of the non-catalyzed versions of the reactions of **1a–c**, which produced isolable amounts of **3a–c**. Accordingly, we supposed that the DDQ-mediated hydrogen abstractions proceed *via* two-step pathways through radical intermediates **9a–c** and **13a–c**, respectively. The non-catalyzed oxidation can also take place *via* cationic intermediates **10a–c** formed by hydride transfer from **1a–c** to DDQ (Scheme 3). Although the overall transformations proved to be favored in terms of thermodynamics (cf. Table 2), the formation of the highly reactive intermediates is endoergic irrespective of their substitution pattern. We assumed that in the presence of ferrocene the reactions of **1a–c** and **2a–c** are initiated by a catalyzed single electron transfer (SET) from the substrate to DDQ with the involvement of Fc/Fc^+ redox pair in a catalytic cycle resulting in intermediate ion pairs **11a–c** and **12a–c** composed of a radical cation and radical anion $DDQ^{\bullet-}$. Although the calculations indicated that for each of the studied models, this type of SET is unfavored in terms of thermodynamics but can probably be considered as kinetically favored due to ferrocene-catalysis that produces **11a–c** and **12a–c** in amount sufficient to maintaining a steady-state further advancing the overall reactions towards completion. The formation of the variety of isolable products was interpreted by branched mechanistic pathways starting from different types of thermodynamically favored exoergic specific collisions of the appropriate radical cation and $DDQ^{\bullet-}$ inside the ion pairs of **11a–c** and **12a–c** (Scheme 3). Two accessible variants for the recombination of **11a–c** generating polycyclic and bicyclic sulfonium phenolate intermediates **19a–c** and **27a–c**, respectively, were analyzed by theoretical modelling. The results indicated that the elementary steps taking place by recombination with concomitant intramolecular cyclizations (**11a–c** → **19a–c)** are exoergic, but based on the calculated enegetic data, the formation of **27a–c** seems even more favored in terms of thermodynamics. On the other hand, both the polycyclic and bicyclic sulfonium intermediates are supposed to be converted into the same ion pairs type **23** by 1,2-elimination-tautomerization sequence **19a–c** → **21a–c** → **23a–c** and sulfonium-mediated intramolecular aromatic electrophilic substitution **27a–c** → **23a–c** [85], respectively. Advancing further along the proposed mechanistic pathway **t**he polycyclic sulfonium intermediates **23a–c** undergo deprotonation-initiated 1,4-elimination accompanied by concomitant skeletal fragmentation (**23a–c** → $DDQH_2$ + **I** + **III** or **IV**). Our calculations identified non-covalent pre-Diels-Alder complexes [86] (**25a** and **25bc**) representing local minima on the potential energy surface as formed by exoergic associations from pyridazino[4,5-*d*]pyridazine **I** and the appropriate aryne intermediate **III** or **IV.** Finally, **25a** and **25bc** undergo Diels-Alder (DA) addition followed by N_2-releasing retro Diels-Alder (rDA) of the resulting bridged intermediates **17a** and **17bc** to afford benzo- and angularly fused naphthophthalazines **5a** and **5bc**, respectively. Minor portions of these phthalazines can also be formed along the multistep pathway

 doi:10.20944/preprints202506.1204.v1

comprising slightly exoergic trans-annular cyclization of the primarily generated radicals **13a–c** followed by H-abstraction-rDA sequence proceeding *via* intermediates type **15** and **17.** However, besides phthalazines, dearylated pyridazino[4,5-*d*]pyridazine **I** was also isolated from the reaction mixtures in yields lower relative to those of phtalazine products (Table 1) pointing to a competition between the formation of pre-Diels-Alder complexes **25a** and **25bc** and other aryne-consuming conversions [87]. Analogous sequence which might lead to pyrazolyl-containing fused phthalazines **6a–c** was also analyzed by theoretical modelling. The calculated energetic values disclose a slightly endoergic character of the trans-annular cyclizations of the primarily generated radicals **14a–c** referring to a decreased feasibility of this type of multistep transformations.

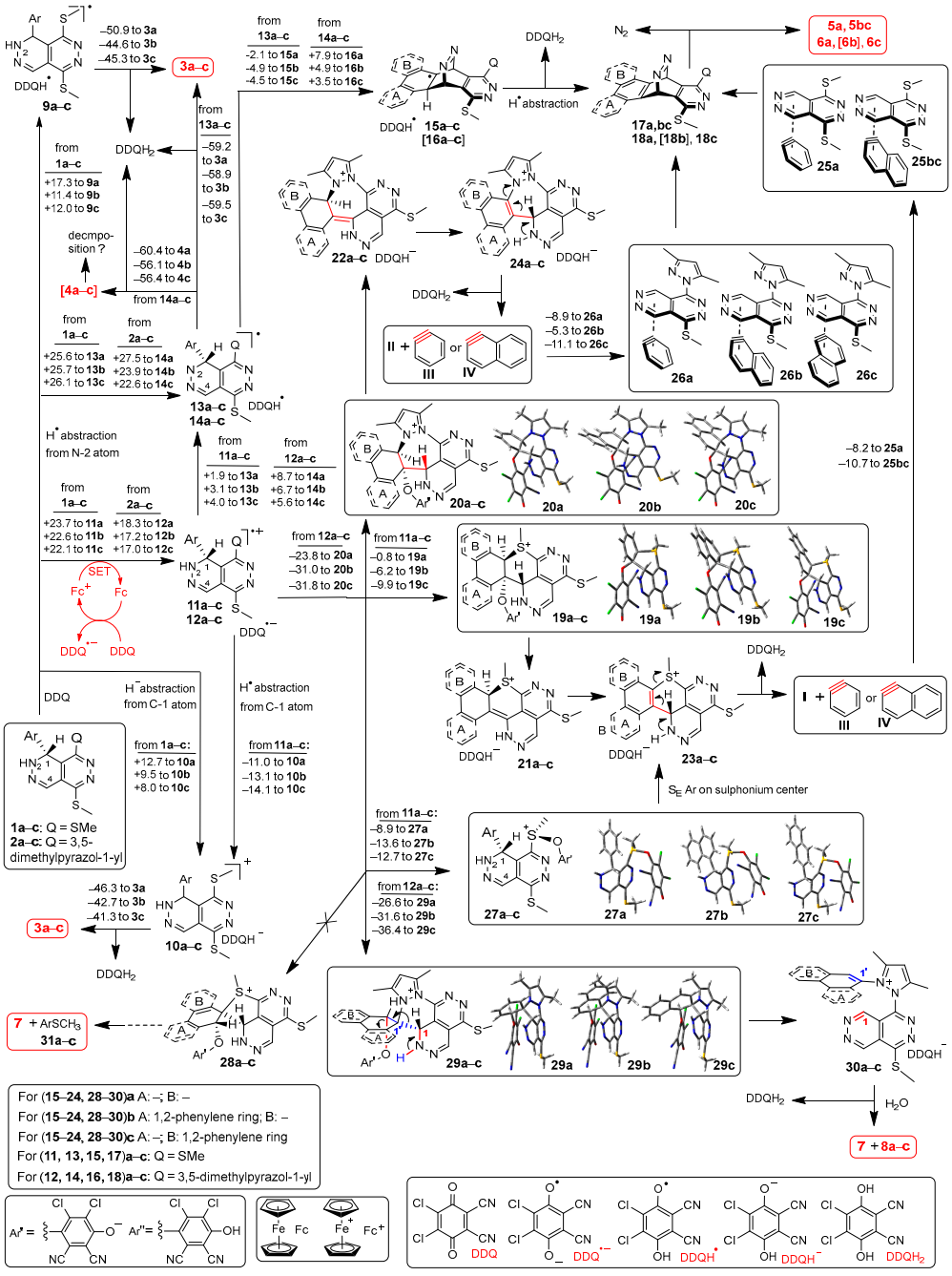

Scheme 3. Summary of the modelling-supported pathways that might lead to the versatile products formed in the dehydroaromatization reactions of selected models **1a–c** and **2a–c**. The ΔG values calculated for the energetics of the elementary steps considereded most relevant to estimating the relative feasibility of the competitive pathways are given in [kcal/mol].

 doi:10.20944/preprints202506.1204.v1

We also carried out modelling studies on two versions of the recombination of appropriate the radical cations and $DDQ^{\bullet-}$ inside ion pairs **12a–c** accompanied by simultaneous intramolecular cyclizations with the involvement of the proximal pyrazolyl and aryl groups generating 1,2-diazepine-fused polyheterocycles **20a–c** and spiroheterocycles **29a–c**. The calculated data shows that both types of cyclization-assisted radical-radical recombination are markedly exoergic processes characterized by comparable changes in energetics. According to our proposed mechanism polyheterocycles **20a–c** undergo elimination of $DDQH^-$ followed by facile tautomerization in the resulting cations associated with rearomatization of the fused carbocyclic ring (**20a–c** → **24a–c**). In the subsequent steps **24a–c** can also be assumed to undergo fragmentation (**24a–c** → $DDQH_2$ + **II** + **III** or **IV**) followed by the formation of pre-Diels-Alder complexes and subsequent DA and rDA reactions finally affording benzo- and naphtho-condensed pyrazolylphthalazines type **6**. It is of particular interest that – according to the changes in the energetics accompanying aryne complexation –the association of **II** and **IV** leading to **26c** is markedly favored over the formation of isomeric complex **26b**. The relative energetics calculated for the alternative association modes of **II** and **IV** provides rationale for the outcome of one of the intriguing synthetic experiments reported in this contribution disclosing that both **2b** and **2c** got converted into **6c**, while **6b** could not be isolated from the mixtures obtained by the reactions of **2b**.

Our modelling studies also found that in a markedly exothermic manner the ion pairs **12a–c** are ready to get converted into spirocyclic intermediates **29a–c** which can be further transformed into **30a–c** by 1,4-eliminiation of $DDQH^-$ taking place by the cleavage of the C1-C1′ bond accompanied by simultaneous aromatization of the heterocycle and the aryl group. In the pathway-terminating step **30a–c** undergo hydrolysis with the water contamination of the solvents used to give heterocyclic lactam **7** and the corresponding 3,5-dimethyl-1-aryl-1*H*-pyrazole type **8**. Due to avoiding the formation of a carbon-sulphur bond in a strained spirocyclic framework with a five-membered ring, the structures of **28a–c** could not be identified as local minima on the potential energy surface (PES) ruling out the collision-assisted spirocyclization of *bis*-methylthio-substituted radical ion pairs **11a–c** and – in keeping with our experimental findings – the final generation of lactam **7** and thioethers **31a–c**.

Finally, in the context of mechanistic pathways we assume that the deprotonation of radical cations type $\mathbf{12}^{+}$ can preferably occur on N-1 atom (cf. the slightly endoergic conversions of **12a–c** → **14a–c**) rather than from position 1 as deprotonation of C-1 is assumed to be sterically hindered by the rapidly double-twisting proximal pyrazolyl ring (according to molecular modelling the full rotation of this bulky substituent with two pending methyl groups is prevented by the sterically congested molecular architecture). Accordingly, the abstraction of hydrogen atom from the C-1 position of **2a–e** is also regarded as sterically hindered, kinetically unfavored elementary step. This view is supported by the H-bond transmitted correlation detected in the ^{1}H-^{15}N-HMBC spectra of compounds type **2** as we reported in earlier [18].

Since **30a–c** were obviously consumed by lactame-generating hydrolysis under the conditions of Methods D–F using solvents without prior absolutization, with the intention of trapping at least one representative of these key intermediates in a related molecular architecture, we reacted **2c** with a sub-equimolar amount of DDQ at 60 °C in absolutized THF (Method G) to facilitate the construction of dimer **32c** (Scheme 4) by a nucleophilic-electrophilic interaction between the portion of **2c** remained intact and cation **30.** In accord with our expectation **32c** could also be isolated in not-negligible yield (16%) from the complex reaction mixture. We also managed to separate naphthophthalazine **6c**, pyrazole **8c** and a THF-derived butoxy-substituted aromatic heterocycle **33** in moderate yields (Scheme 4a). Besides these products a small amount (10%) of unreacted **2c** was also recovered from the crude reaction mixture. With this experience in hand, disclosing the feasibility of the formation of a coupled heterocycle such as **32c**, using equimolar amounts of **1c** and **2c** we also performed a cross experiment under the conditions of Method G (Scheme 4b) to check indirectly whether the DDQ-mediated ferrocene-catalyzed primary oxidation of **2c**, taking place *via* SET, thermodynamically is favoured over that of **1c**, as suggested by the changes in the free energy

 doi:10.20944/preprints202506.1204.v1

(ΔG = +22.1 kcal/mol and + 17.0 kcal/mol calculated for elementary steps **1c** → **11c** and **2c** → **12c**, respectively (Scheme 3). It must be pointed out here that in spite of their endoergic character, the overall feasibility of these SET processes are presumably significantly increased by the involvement of ferrocene as an efficient redox catalyst. Thus, we hypothesized that the aforementioned difference in thermodynamics would eventually facilitate the selective formation of cation **30c** which can react with the unchanged portion of **1c** to give the coupled product **34c** (Scheme 3). This hypothesis got supported by the outcome of the experiment: besides **6c**, **8c** and **33** derived from **2c** and a small amount of **3c** derived from a partial dehydroaromatization of **1c**, **34c** could also be isolated in moderate yield (19%).

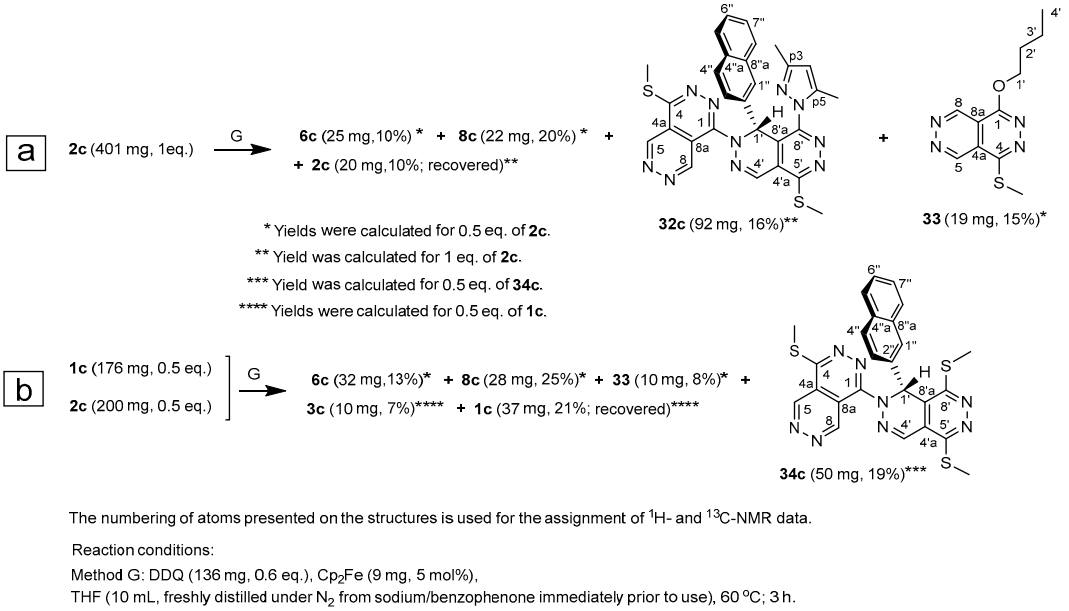

Scheme 4. a.) Experiment using sub-equimolar DDQ performed with the intention of trapping the cationic intermediate **30c** (cf. Scheme 3) in the dimer product **32c**. **b**.) A dimer-generating cross experiment using sub-equimolar DDQ to assess indirectly the relative propensity of **1c** and **2c** to undergo oxidation in the ferrocene-catalyzed SET process.

Based on the results of further modelling studies we suggest that under the conditions of Method G an endoergic solvolysis of cation **30c**, effected by the excess of the solvent molecules, generates cationic intermediate **35** of which highly exoergic displacement reactions with the intact portions of **2c** and **1c** give **32c** and **34c**, respectively (Scheme 5). The formation of **33** can be interpreted by an exoergic hydride-transfer from a THF molecule opening the five-membered oxonium ring in **35**.

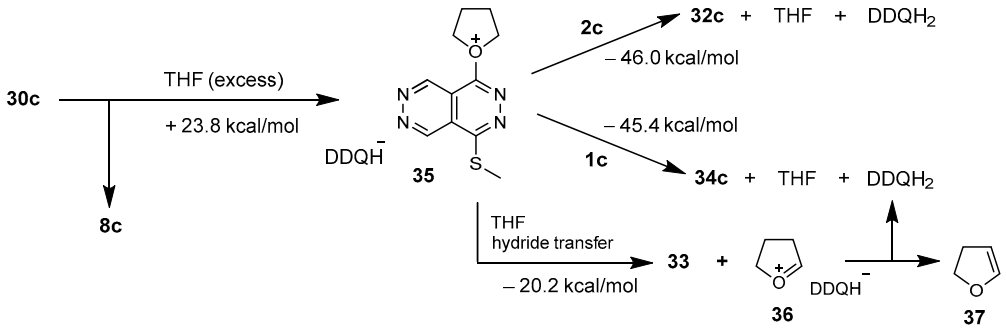

Scheme 5. The modelling-supported mechanism proposed for the THF-promoted formation of coupled products **32c** and **34c** and butoxy-substituted pyridazino[4,5-*d*]pyridazine **33** from the cationic intermediate **30c**.

 doi:10.20944/preprints202506.1204.v1

As exemplified by the regioselective transformations of radical ion pairs **11a** and **12a** (Scheme 3) we have also performed further modelling studies to reveal the spatial distribution of the relevant delocalized molecular orbitals (MOs) of representative radical cations **11a**$^{+}$ and **12a**$^{+}$ determining the pathways to the isolated products (Scheme 6).

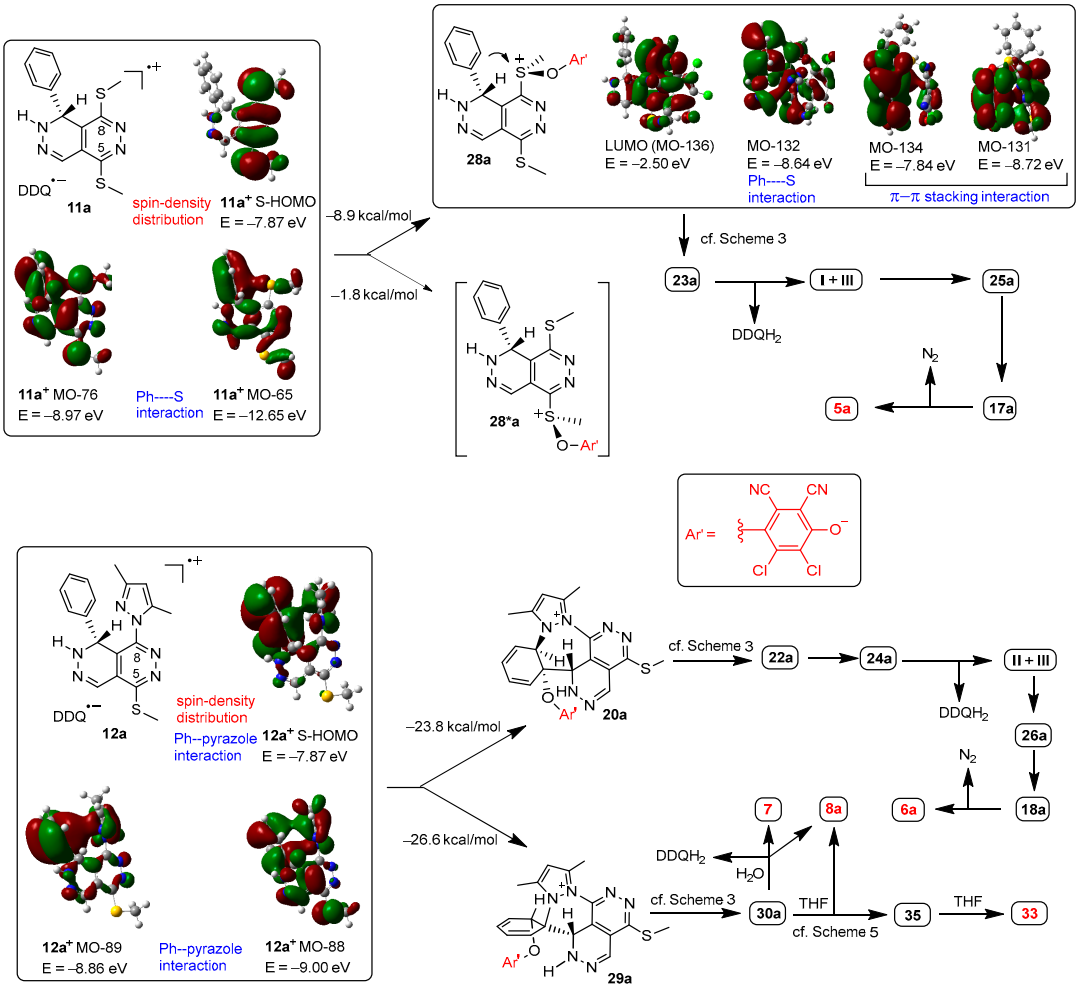

Scheme 6. Modelling-supported MO-based rationalization of the regioselectivity of the cyclization-assisted radical colligations of the radical ion pair types **11** and **12** leading to different products, as visualized by the most relevant MOs of the representative radical cations **11a**$^{+}$ and **12a**$^{+}$.

The singly occupied MO of **11a**$^{+}$ was found to be delocalized along the *bis*-methylthio-substituted aromatic pyridazine ring with substantial, but comparable shares on the two sulphur centres attached to C-8 and C-5 suggesting at first sight a balanced competition under an assumed kinetic control between the two modes of recombination constructing sulphonium phenolates **28a** and **28a***, respectively. However, the calculated energetic values identified **11a** → **28a** as the process which is thermodynamically favoured over the alternative coupling **11a** → **28a*.** It is of note that in cation **11a**$^{+}$ the bonding MOs 88 and 89 indicate a marked phenyl-sulphur interaction which can be considered as a contributing factor increasing the feasibility of the sulphonium-generation in the S-methyl group on position 8. In this context the MO analysis of **28** disclosed a substantial share of the LUMO on the sulphonium centre implicated in an interaction with the proximal π-donor phenyl group (cf. MO-132) preformed for the cyclization yielding **23** of which subsequent multistep conversion finally leads to the formation of benzophthalazine **5a** (Schemes 3 and 6). On the other hand, MO analysis of **28** also identified two bonding orbitals (MO-131 and MO-134) that represent a substantial π–π stacking interaction between the nearly parallel aromatic carbocyclic- and heterocyclic fragments contributing to the overall stability of the molecular architecture.

 doi:10.20944/preprints202506.1204.v1

Underlying the proposed mechanistic pathways starting from radical ion pair **12** (Scheme 3), the singly occupied MO of cation **12a**$^{+}$ was found to be delocalized over the proximal interacting pyrazolyl- and phenyl substituents with larger spin density on the phenyl ring. On the other hand, the electron-delocalization between the interacting rings visualized by MOs 88 and 89 is assumed to assist the alternative modes of cyclization that necessarily accompany the colligation of the radical ion pair taking place on the phenyl ring (Schemes 3 and 6). It must also be emphasized here that in satisfactory agreement with the ratio of the yields of benzophthalazine **6a** and lactame **7** (Table 1, entry 6), the two readily isolable representative products formed by two distinct mechanisms, the competing cyclization-assisted exoergic colligations **12a** → **20a** and **12a** → **29a** can be characterized by comparable thermodynamics as reflected from the calculated data (Schemes 3 and 6).

Since the protocols applied for the dehydroaromatization of **1d**,**e** and **2d**,**e** provided product distributions markedly different from those obtained by the analogous reactions of **1a–c** and **2a–c** (Table 1) the energetic profile of the possible competitive pathways of their multistep transformations were also analyzed focusing on the cascade-initiating steps that determine the direction of the overall transformations (Scheme 7). The exclusive formation of **3d** from **1d** can be reasoned by comparison of the energetics of the highly favored hydrogen abstraction **11d** → **10d** and the much less exoergic S-O colligation **11d** → **27d**. It is obvious that due to a conjugation effect the 4-methoxyphenyl group substantially enhances the stability of cation **10d**$^{+}$. On the other hand, in line with the dominant formation of **3e** and the low, but reproducible yields of **I** (Table 3), we calculated somewhat more balanced energetics for the competitive transformations **11e** → **10e** and **11e** → **27e.** It is important to mention that competitive couplings **11a–c** → **10a–c** and **11a–c** → **27a–c** can be characterized by relatively balanced energetics starting branched pathways finally constructing products **3a–c** and **5a,bc** (Scheme 3) in comparable isolated yields (Table 1). However, the aryne intermediates **V** and **VI** are assumed to undergo uncontrolled transformations rather than being involved in DA-rDA sequence terminating the pathway (cf. Scheme 3) started by S-O colligation **11e** → **27e**.

The pyrazole-containing radical ion pair **12d** undergoes a highly exoergic colligation assisted by the formation of spirocyclic intermediate **29d** of which hydrolysis-terminated multistep conversion leads to lactame **7** and pyrazole **8d**, the products isolated in mediocre but comparable yields (Table 1). Probably due to the significant difference in the energetics of the alternative cascade-initiating steps **12d** → **29d** and **12d** → **20d** none of the reactions of **2d** led to the formation of **II**. On the other hand, the highly exoergic colligation **12e** → **20e** is efficiently assisted by the formation of a polyheterocyclic skeleton comprising a thieno[3,2-*c*][1,2]diazepine subunit with combination of fused five- and seven-membered rings, which presumably accumulates less inherent strain compared to benzo[c][1,2]diazepines [in **20a** (Scheme 3), **20d** (Scheme 7)], naphtho[2,1-*c*][1,2]diazepine and naphtho[1,2-*c*][1,2]diazepine [in **20b** and **20c**, respectively (Scheme 3)] generated by combination of fused six- and seven-membered rings [88]. Based on the mechanistic considerations outlined in Scheme 3, the multistep transformation of **20e** is expected to be terminated by a fragmentation resulting in **II** and the five-membered heteroarene **VI** which, avoiding the formation of a pre-Diels-Alder complex, presumably undergoes fast aryne-consuming conversions [87]. Thus, the formation of II in the reactions of 2d as exclusive product isolable in relatively high yields (Table 1) is in accord with the relative energetics calculated for the cyclization-assisted colligation **12e** → **20e** and the less favored spirocyclization formation of the spirocyclic intermediate **12e** → **29e** (Scheme 7).

The ^{1}H- and ^{13}C NMR data of the novel 1,4-bis(methylthio)-5-aryl-py- ridazino[4,5-d]pyridazines 3a–e, benzo- and naphtho-condensed phthalazines types 5 and 6, lactame 7 pyrazoles type 8, butyl ether 33 and coupled products 32c and 34c are consistent with their structures, but the following remarks are necessary to make.

 doi:10.20944/preprints202506.1204.v1

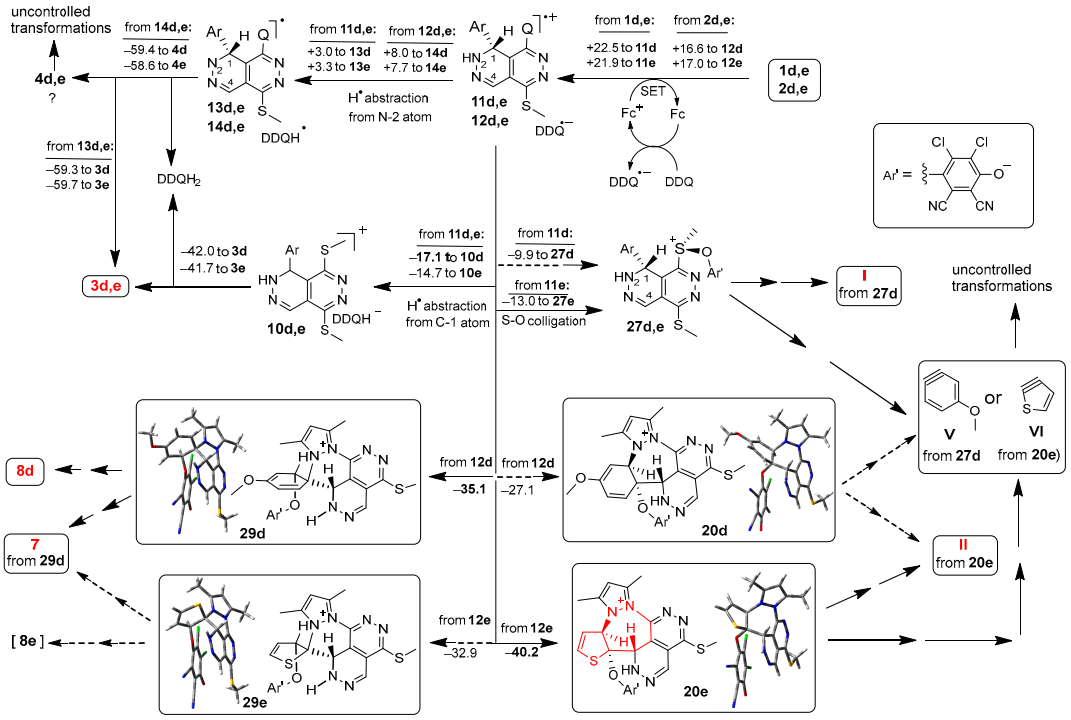

Scheme 7. Modelling-supported interpretation of the multistep transformations of **3d**,**e** and **4d**,**e**, leading to product distributions somewhat different from those obtained by the related reactions using **1a–c** and **2a–c** as precursors**.**

In the ^{1}H-^{13}C-HMBC spectrum of 6c the H-12 singlet shows a three-bond correlation with the C-11 signal identified through its interaction with the protons of the methylthio group. Finally, besides the coupling pattern of the protons on the aromatic ring, the characteristic NOE interaction detected between protons H-1 and H-12 proves the angular arrangement of the tetracyclic skeleton of this naphtho-condensed phthalazine.

In the ^{1}H-NMR spectrum of 32c the H-1′ signal is highly downfield-shifted (to 8.06 ppm) due to the cooperative anisotropic deshielding effects exerted by the proximal N-2 and N-p2 atoms situated in the bicyclic heteroaromatic aromatic skeleton and the pyrazole ring, respectively. The H-1′ signal of 34c discernible at 7.65 ppm is less, yet significantly downfield-shifted referring to a decreased degree of anisotropic effect exerted by the N-2 atom. However, it is the diagnostic three-bond correlation between H-1′ and C-1 atoms detected by the ^{1}H-^{13}C-HMBC spectra of 32c and 34c, which provides unequivocal evidence of the connection between the two heterocyclic fragments in their molecular architecture. The constitution of 34c gained an additional support from a ^{1}H-^{15}N-HMBC measurement [reference: δ(NH_3) = 0 ppm] indirectly detecting N-6 and N-7 resonances as identified at 396 ppm *via* their unresolved cross-peaks with H-5 and H-8 signals, N-3′ resonance at 335 ppm, as identified *via* its cross-peak with the H-1′ signal and N-2′ resonance at 155 ppm, as identified *via* its cross-peak also with the H-1′ signal.

4. Materials and Methods

All fine chemicals were obtained from commercially available sources (Merck, Budapest, Hungary, Molar Chemicals, Budapest, Hungary, VWR, Budapest, Hungary) and were used without further purification. Tetrahydrofuran (THF) was freshly distilled under N_2 from sodium/benzophenone immediately prior to use under the conditions of Method G. Merck Kieselgel (230–400 mesh, 60 Å) was used for flash column chromatography. To achieve sufficient separation of the multiple products, the ratio of the separable mixture to silica was set at least to 1 g:100 g). Melting points (uncorrected) were determined with a M-560 instrument (Büchi, Essen, Germany). Elemental analyses were performed by a PerkinElmer 2400 CHNS elemental analyzer. Merck Kieselgel 60F254

 doi:10.20944/preprints202506.1204.v1

plates were used for TLC monitoring the reaction mixtures. The NMR spectra were recorded in DMSO-d_6 or $CDCl_3$ solution in 5 mm tubes at RT, on a Bruker DRX-500 spectrometer (Bruker Biospin, Karlsruhe, Baden Württemberg, Germany) at 500 (^{1}H), 125 (^{13}C) and 50 (^{15}N) MHz, with the deuterium signal of the solvent as the lock and TMS as internal standard (^{1}H, ^{13}C) and NH_3(liq.) as external reference (^{15}N). The ^{15}N NMR chemical shifts of compound **34c** were assigned on the basis of the correlations revealed by its ^{1}H-^{15}N HMBC spectrum. The ^{1}H-^{1}H-COSY, ^{1}H-^{13}C-HSQC, ^{1}H-^{13}C-HMBC and ^{1}H-^{15}N-HMBC spectra were registered by using the standard Bruker pulse programs The energetic profile of the transformations was given by the changes in Gibbs free energy (ΔG). The free energy values of the optimized structures were obtained by correcting the computed total energy with zero-point vibrational energy (ZPE) and thermal corrections. All calculations were carried out using the Gaussian 09 software (Gaussian Incorporation, Pittsburgh, USA) package [89]. The optimized structures are available from the authors.

4.1. General Procedure for the Dehydroaromatization of 1a–e and 2a–e Effected by DDQ Under the Conditions of Methods A-F

At room temperature DDQ (545 mg, 2.4 mmol, 1.2 equiv.) was added to the solution of 1-aryl-1,2-dihydropyridazino[4,5-*d*]pyridazine (2 mmol) in 20 mL of the solvent (MeCN by Methods A and D; THF by Methods B and E; DMSO by Methods C and F). When the reactions were conducted under the conditions of Methods D–E, prior to addition of DDQ, ferrocene (18.6 mg, 0.1 mmol) was also dissolved in the reaction mixture. All reaction mixtures were stirred under argon at 60 °C for 5 h (Methods A-C) or 3 h (Methods D-F) (cf. Scheme 2). After the stirring was stopped, the mixture was allowed to cool down to room temperature and quenched with saturated $NaHCO_3$ solution (10 mL) then diluted with water (100 mL). The resulting suspension was extracted with CH_2Cl_2 (5x40 mL). The combined organic layers were washed with brine, dried over Na_2SO_4, passed through a Celite pad and concentrated to dryness. The brown thick oily residue was triturated with water. The resulting solid was filtered off, dried and subjected to flash column chromatography on silica gel using petroleum ether/EtOAc (80:1−20:1, v/v) as eluent. The separated products were further purified by trituration with hexane/Et_2O (3:1−1:1, v/v). The yields of the products are listed in Table 1.

4.2. Procedure for the Reaction of 2c Effected by a Sub-Equimolar Amount of DDQ Under the Conditions of Method G

At room temperature ferrocene (9 mg, 5 mol%) and DDQ (136 mg, 0.6 mmol, 0.6 equiv.) were sequentially added to the solution of **2c** (401 mg, 1 mmol, 1 equiv.) in THF (10 mL) distilled freshly under N_2 from sodium/benzophenone. The reaction mixture was stirred under argon at 60 °C for 3 h. After the stirring was stopped, the mixture was allowed to cool down to room temperature and quenched with saturated $NaHCO_3$ solution (5 mL) then diluted with water (50 mL). The resulting suspension was extracted with CH_2Cl_2 (5x20 mL). The combined organic layers were washed with brine, dried over Na_2SO_4, passed through a Celite pad and concentrated to dryness. The resulting brown thick oil was triturated with water to obtain the mixture of the crude products of which were separated and further purified by procedure described in subsection 5.1. The yields of the products are presented in Scheme 4a.

4.3. Procedure for the Reaction of a 1:1 Mixture of 1c and 2c Effected by a Sub-Equimolar Amount of DDQ Under the Conditions of Method G

At room temperature ferrocene (9 mg, 5 mol%) and DDQ (136 mg, 0.6 mmol, 0.6 equiv.) were sequentially added to the mixture of **1c** (176 mg, 0.5 mmol, 0.5 equiv.) and **2c** (200 mg, 0.5 mmol, 0.5 equiv.) dissolved in THF (10 mL) distilled freshly under N_2 from sodium/benzophenone. The reaction mixture was stirred under argon at 60 °C for 3 h. After the stirring was stopped, the mixture was allowed to cool down to room temperature and quenched with saturated $NaHCO_3$ solution (5 mL) then diluted with water (50 mL). The resulting suspension was extracted with CH_2Cl_2 (5x20 mL). The

 doi:10.20944/preprints202506.1204.v1

combined organic layers were washed with brine, dried over Na_2SO_4, passed through a Celite pad and concentrated to dryness. The resulting thick brown oil was triturated with water to obtain the mixture of the crude products of which were separated and further purified by procedure described in subsection 5.1. The yields of the products are presented in Scheme 4b.

4.4. Characterization of the Products

4.4.1. 1,4-bis(methylthio)-5-phenylpyridazino[4,5-d]pyridazine (**3a**)

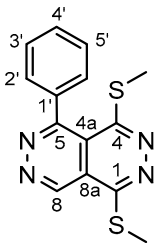

White powder. M.p. 133-134 °C. ^{1}H-NMR ($CDCl_3$): 9.85 (s, 1H, H-8); 7.63 (m, 1H, H-4′); 7.60-7.52 (overlapping m's, 4H, H-2′,6′ and H-3′,5′); 2.90 (s, 3H, SC<u>H</u>$_3$ on C-1); 2.54 (s, 3H, SC<u>H</u>$_3$ on C-4). ^{13}C-NMR ($CDCl_3$): 158.2 (C-5); 157.3 (C-4); 156.4 (C-1); 145.7 (C-8); 136.4 (C-1′); 130.8 (C-4′); 130.5 (C-3′,5′); 128.9 (C-2′,6′); 119.0 (C-4a); 117.0 (C-8a); 15.9 (S<u>C</u>H$_3$ on C-4); 13.6 (S<u>C</u>H$_3$ on C-1). Anal. calcd. for $C_{14}H_{12}N_4S_2$: C 55.98%; H, 4.03%; N, 18.65%; S, 21.35%. Found: C, 55.83%; H, 4.11%; N, 18.81%; S, 21.28%.

4.4.2. 1,4-Bis(methylthio)-5-(naphthalen-1-yl)pyridazino[4,5-d]pyridazine (**3b**)

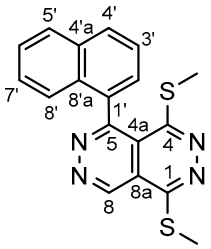

White powder. M.p. 177-180 °C. ^{1}H-NMR ($CDCl_3$): 9.97 (s, 1H, H-8); 8.14 (d, *J* = 8.1 Hz, 1H, H-4′); 8.00 (d, *J* = 8.1 Hz, 1H, H-5′); 7.66 (dd, *J* = 8.1 Hz and 7.7 Hz, 1H, H-3′); 7.56 (dd, *J* = 8.4 Hz and 7.7 Hz, 1H, H-6′); 7.52 (d, *J* = 7.4 Hz, 1H, H-2′); 7.41 (dd, *J* = 8.4 Hz and 7.7 Hz, 1H, H-7′); 7.20 (d, *J* = 8.4 Hz, 1H, H-8′); 2.91 (s, 3H, SC<u>H</u>$_3$ on C-1); 2.36 (s, 3H, SC<u>H</u>$_3$ on C-4). ^{13}C-NMR ($CDCl_3$): 157.4 (C-5); 157.0 (C-4); 156.1 (C-1); 145.9 (C-8); 133.5 (C-4′a); 133.2 (C-1′); 132.5 (C-8′a); 130.9 (C-4′); 129.0 (C-2′); 128.5 (C-5′); 127.2 (C-7′); 126.5 (C-6′); 125.3 (C-3′); 124.7 (C-8′); 118.4 (C-4a); 117.9 (C-8a); 15.6 (S<u>C</u>H$_3$ on C-4); 13.3 (S<u>C</u>H$_3$ on C-1). Anal. calcd. for $C_{18}H_{14}N_4S_2$: C 61.69%; H, 4.03%; N, 15.99%; S, 18.30%. Found: C, 61.50%; H, 4.15%; N, 15.80%; S, 18.42%.

4.4.3. 1,4-Bis(methylthio)-5-(naphthalen-2-yl)pyridazino[4,5-d]pyridazine (**3c**)

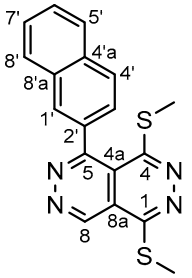

 doi:10.20944/preprints202506.1204.v1

White powder. M.p. 199-201 °C. ^{1}H-NMR ($CDCl_3$): 9.85 (s, 1H, H-8); 8.14 (d, *J* = 8.1 Hz, 1H, H-4′); 8.03 (overlapping br s and d, *J* = 8.1 Hz, 2H, H-1′ and H-4′, respectively); 7.96 (d, *J* = 8.2 Hz, 1H, H-5′); 7.93 (d, *J* = 8.4 Hz, 1H, H-8′); 7.66 (dd, *J* = 8.1 Hz and 1.5 Hz, 1H, H-3′); 7.61 (dd, *J* = 8.2 Hz and 7.7 Hz, 1H, H-6′); 7.58 (dd, *J* = 8.4 Hz and 7.7 Hz, 1H, H-7′); 2.88 (s, 3H, SC$\underline{H}_3$ on C-1); 2.45 (s, 3H, SC$\underline{H}_3$ on C-4). ^{13}C-NMR ($CDCl_3$): 158.3 (C-5); 157.5 (C-4); 156.4 (C-1); 145.6 (C-8); 134.5 (C-4′a); 133.8 (C-2′); 133.2 (C-8′a); 131.2 (C-1′); 129.2 (C-8′); 128.8 (C-4′); 128.4 (C-5′); 128.0 (C-6′); 127.3 (C-7′); 127.1 (C-3′); 119.2 (C-4a); 117.2 (C-8a); 15.9 (S$\underline{C}$H$_3$ on C-4); 13.6 (S$\underline{C}$H$_3$ on C-1). Anal. calcd. for $C_{18}H_{14}N_4S_2$: C, 61.69%; H, 4.03%; N, 15.99%; S, 18.30%. Found: C, 61.48%; H, 3.94%; N, 16.10%; S, 18.37%.

4.4.4. 5-(4-Methoxyphenyl)-1,4-bis(methylthio)pyridazino[4,5-d]pyridazine (**5d**)

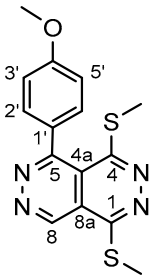

Light yellow powder. M.p. 182-184 °°C. ^{1}H-NMR ($CDCl_3$): 9.78 (s, 1H, H-8); 7.49 (d, *J* = 8.1 Hz, 2H, H-2′,4′); 7.08 (d, *J* = 8.1 Hz, 2H, H-3′,5′); 3.93 (s, 3H, OC$\underline{H}_3$ on C-4′); 2.87 (s, 3H, SC$\underline{H}_3$ on C-1); 2.54 (s, 3H, SC$\underline{H}_3$ on C-4). ^{13}C-NMR ($CDCl_3$): 161.7 (C-4′); 157.7 (C-5); 157.1 (C-4); 155.9 (C-1); 144.9 (C-8); 131.8 (C-2′,6′); 128.2 (C-3′,5′); 118.8 (C-4a); 116.7 (C-8a); 55.5 (O$\underline{C}$H$_3$ on C-4′); 15.5 (S$\underline{C}$H$_3$ on C-4); 13.2 (S$\underline{C}$H$_3$ on C-1). Anal. calcd. for $C_{15}H_{14}N_4OS_2$: C, 54.53%; H, 4.27%; N, 16.96%; S, 19.41%. Found: C, 54.70%; H, 4.41%; N, 17.13%; S, 19.52%.

4.4.5. 1,4-Bis(methylthio)-5-(thiophen-2-yl)pyridazino[4,5-d]pyridazine (**3e**)

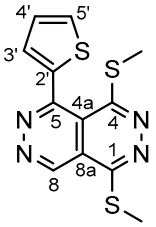

Light yellowish powder. M.p. 136-138 °C. ^{1}H-NMR ($CDCl_3$): 9.80 (s, 1H, H-8); 7.72 (d, *J* = 4.6 Hz, 1H, H-5′); 7.38 (d, *J* = 2.7 Hz, 1H, H-3′); 7.24 (dd, *J* = 4.6 Hz and 2.7 Hz, 1H, H-4′); 2.89 (s, 3H, SC$\underline{H}_3$ on C-1); 2.59 (s, 3H, SC$\underline{H}_3$ on C-4). ^{13}C-NMR ($CDCl_3$): 157.2 (C-4); 156.2 (C-1); 152.6 (C-5); 145.6 (C-8); 135.9 (C-2′); 133.7 (C-3′); 130.9 (C-5′); 128.1 (C-4′); 119.2 (C4a); 117.7 (C-8a); 15.8 (S$\underline{C}$H$_3$ on C-4); 13,6 (S$\underline{C}$H$_3$ on C-1). Anal. calcd. for $C_{12}H_{10}N_4S_3$: C, 47.04%; H, 3.29%; N, 18.28%; S, 31.39%. Found: C, 47.21%; H, 3.32%; N, 18.09%; S, 31.23%.

4.4.6. 1,4-Bis(methylthio)benzo[g]phthalazine (**5a**)

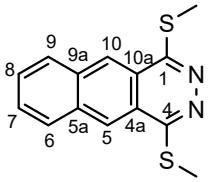

 doi:10.20944/preprints202506.1204.v1

Light yellowish powder. M.p. 184-186 °C. ^{1}H-NMR ($CDCl_3$): 8.65 (s, 2H, H-5,10); 8.12 (m, 2H, H-6,9); 7.69 (m, 2H, H-7,8); 2.83 (s, 6H, SC<u>H</u>$_3$). ^{13}C-NMR ($CDCl_3$): 158.6 (C-1,4); 135.1 (C-5a, 9a); 129.5 (C-6,9); 128.9 (C-7,8); 124.7 (C-5,10); 122.2 (C-4a,10a); 13.5 (S<u>C</u>H$_3$). Anal. calcd. for $C_{14}H_{12}N_2S_2$: C, 61.73%; H, 4.44%; N, 10.28%; S, 23.54%. Found: C, 61.52%; H, 4.60%; N, 10.17%; S, 23.60%.

4.4.7. 8,11-Bis(methylthio)naphtho[1,2-g]phthalazine (**5bc**)

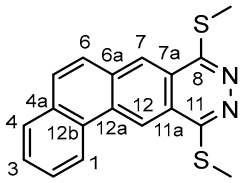

Light yellowish powder. M.p. 198-201 °C. ^{1}H-NMR ($CDCl_3$): 9.19 (s, 1H, H-12); 8.72 (br d, J = 7.7 Hz, 1H, H-1); 8.41 (s, 1H, H-7); 7.88 (br d, J = 7.7 Hz, 1H, H-4); 7.79 and 7.71 (A and B part of an *AB* spin system, J_{AB} = 9.1 Hz, 2x1H, H-6 and H-5, respectively); 7.74 (td, J = 7.7 Hz and 1.5 Hz, 1H, H-2); 7.70 (td, J = 7.7 Hz and 1.5 Hz, 1H, H-3); 2.85 (s, 3H, SC<u>H</u>$_3$ on C-8); 2.87 (s, 3H, SC<u>H</u>$_3$ on C-11). ^{13}C-NMR ($CDCl_3$): 157.9 (C-8); 157.6 (C-11); 134.3 (C-6a); 132.9 (C-12b); 132.4 (C-4a); 130.6 (C-5); 129.6 (C-12a); 129.0 (C-4); 128.6 (C-3); 127.7 (C-2); 126.5 (C-6); 125.6 (C-7); 123.4 (C-1); 122.1 (C-7a); 122.0 (C-11a); 118.3 (C-12); 13.2 (s, 3H, SC<u>H</u>$_3$ on C-8); 13.1 (s, 3H, SC<u>H</u>$_3$ on C-11). Anal. calcd. for $C_{18}H_{14}N_2S_2$: C, 67.05%; H, 4.38%; N, 8.69%; S, 19.89%. Found: C, 66.90%; H, 4.46%; N, 8.77%; S, 19.92%.

4.4.8. 1-(3,5-Dimethyl-1H-pyrazol-1-yl)-4-(methylthio)benzo[g]phthalazine (**6a**)

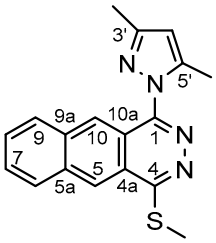

Light yellow powder. M.p. 206-207 °C. ^{1}H-NMR ($CDCl_3$): 8.85 (s, 1H, H-10); 8.77 (s, 1H, H-5), 8.17 (d, J=7.8 Hz, 1H, H-6); 8.12 (d, J=7.8 Hz, 1H, H-9); 7.73 (t, J=7.8 Hz, 1H, H-7); 7.69 (t, J=7.8 Hz, 1H, H-8);); 6.19 (s, 1H, H-4'); 2.93 (s, 3H, SC<u>H</u>$_3$); 2. 52 (s, 3H, C<u>H</u>$_3$ on C-5'); 2.43 (s, 3H, C<u>H</u>$_3$ on C-3'). ^{13}C-NMR ($CDCl_3$): 161.5 (C-4); 151.13 (C-3'); 151.08 (C-1); 143.3 (C-5'); 135.5 (C-9a); 135.0 (C-5a); 130.0 (C-9); 129.3 (C-6); 129.2 (C-7);128.8 (C-6); 128.0 (C-10); 124.8 (C-4a); 124.0 (C-5); 119.7 (C-10a); 108.1 (C-4'); 14.2 (<u>C</u>H$_3$ on C-3'); 13.6 (S<u>C</u>H$_3$), 12.9 (<u>C</u>H$_3$ on C-5'). Anal. calcd. for $C_{18}H_{16}N_4S$: C, 67.47%; H, 5.03%; N, 17.49%; S, 10.01%. Found: C, 67.65%; H, 5.12%; N, 17.55%; S, 9.94%.

4.4.9. 8-(3,5-Dimethyl-1H-pyrazol-1-yl)-11-(methylthio)naphtho[1,2-g]phthalazine (**6c**)

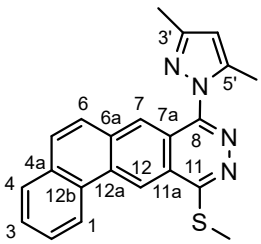

Yellowish powder. M.p. 232-235 °C. ^{1}H-NMR ($CDCl_3$): 9.49 (s, 1H, H-12); 8.90 (br d, J = 8.1 Hz, 1H, H-1); 8.78 (s, 1H, H-7); 7.93 (br d, J=8.0 Hz, 1H, H-1); 7.86 and 7.84 (A and B part of an AB spin system, J_{AB} = 9.2 Hz, 2x1H, H-5 and H-6, respectively); 7.80 (t, J = 8.0 Hz, 1H, H-2); 7.75 (t, J = 8.0 Hz,

 doi:10.20944/preprints202506.1204.v1

1H, H-3); 6.18 (s, 1H, H-4′); 2.96 (s, 3H, SC<u>H</u>$_3$); 2. 52 (s, 3H, C<u>H</u>$_3$ on C-5′); 2.43 (s, 3H, C<u>H</u>$_3$ on C-3′). ^{13}C-NMR (CDCl$_3$): 161.4 (C-11); 151.2 (C-3′); 150.9 (C-8); 142.3 (C-5′); 135.4 (C-6a), 133.7 (C-12a); 133.1 (C-4a); 130.6 (C-5); 130.1 (C-12b); 129.5 (C-4); 129.3 (C-3); 128.2 (C-2); 127.6 (C-6); 127.3 (C-7); 125.4 (C-11a); 124.1 (C-1); 120.4 (C-7a); 118.4 (C-12); 108.2 (C-4′); 14.2 (<u>C</u>H$_3$ on C-3′); 13.8 (S<u>C</u>H$_3$), 12.9 (<u>C</u>H$_3$ on C-5′). Anal. calcd. for $C_{22}H_{18}N_4S$: C, 71.33%; H, 4.90%; N, 15.12%; S, 8.65%. Found: C, 71.60%; H, 4.99%; N, 15.25%; S, 8.71%.

4.4.10. 4-(Methylthio)pyridazino[4,5-d]pyridazin-1(2H)-one (**7**)

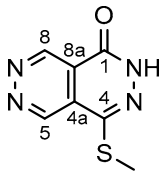

Yellow powder. M.p. 289-293 °C. ^{1}H-NMR (DMSO-*d*$_6$): 13.47 (s, 1H, NH); 9.84 (s, 1H, H-8); 9.71 (s, 1H, H-5); 2.57 (s, 3H, SC<u>H</u>$_3$). ^{13}C-NMR (DMSO-*d*$_6$): 157.0 (C-1); 147.9 (C-8); 146.5 (C-5); 142.2 (C-4); 124.3 (C-4a); 121.8 (C-8a); 12.9 (S<u>C</u>H$_3$). Anal. calcd. for $C_7H_6N_4OS$: C, 43.29%; H, 3.11%; N, 28.85%; S, 16.51%. Found: C, 43.20%; H, 3.19%; N, 28.61%; S, 16.44%.

4.4.11. 3,5-dimethyl-1-phenyl-1H-pyrazole (**8a**)

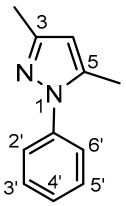

Thick light yellow oil. ^{1}H-NMR (DMSO-*d*$_6$): 7.47 (d, J = 4.2 Hz, 4H, H-2′,3′,5′,6′); 7.37 (m, 1H, H-4′) 6.06 (s, 1H, H-4); 2.28 (s, 3H, C<u>H</u>$_3$ on C-3); 2.19 (s, 3H, C<u>H</u>$_3$ on C-5). ^{13}C-NMR ^{13}C-NMR (DMSO-*d*$_6$): 148.3 (C-3); 140.2 (C-1′); 139.5 C-5); 129.5 (C-3′,5′); 127.3 (C-4′); 124.5 (C-2′,6′); 13.7 (<u>C</u>H$_3$ on C-5); 12.6 (<u>C</u>H$_3$ on C-3). Anal. calcd. for $C_{11}H_{12}N_2$: C, 76.71%; H, 7.02%; N, 16.27%. Found: C, 76.47%; H, 7.29%; N, 16.40%.

4.4.12. 3,5-Dimethyl-1-(naphthalen-1-yl)-1H-pyrazole (**8b**)

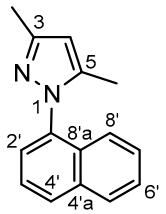

Thick light yellow oil. ^{1}H-NMR (CDCl$_3$): 7.95 (d, *J* = 8.1 Hz, 1H, H-8′); 7.95 (d, *J* = 8.1 Hz, 1H, H-5′); 7.58–7.48 (overlapping m's, 4H, H-2′,3′,6′,7′); 7.36 (d, *J* = 7.9 Hz, 1H, H-4′); 6.10 (s, 1H, H-4); 2.39 (s, 3H, C<u>H</u>$_3$ on C-3); 2.08 (s, 3H, C<u>H</u>$_3$ on C-5). ^{13}C-NMR (CDCl$_3$): 149.0 (C-3); 141.5 (C-5); 136.2 (C-1′); 134.2 (C-4′a); 130.9 (C-8′a); 125.4 (C-2′); 125.1 (C-8′); 123.2 (C-4′); 129.3 (C-5′); 127.3 (C-6′); 128.1 (C-3′); 126.6 (C-7′); 105.4 (C-4); 13.7 (<u>C</u>H$_3$ on C-5); 11.4 (<u>C</u>H$_3$ on C-3). Anal. calcd. for $C_{15}H_{14}N_2$: C, 81.05%; H, 6.35%; N, 12.60%. Found: C, 81.38%; H, 6.49%; N, 12.36%.

4.4.13. 3,5-Dimethyl-1-(naphthalen-2-yl)-1H-pyrazole (**8c**)

 doi:10.20944/preprints202506.1204.v1

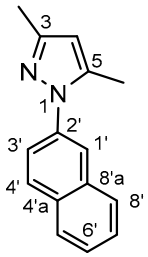

Thick yellow oil. ^{1}H-NMR (DMSO-d_6): 8.05–8.00 (three overlapping signals: two d's J = 8.9 Hz and 8.1 Hz, and a br s, 3H, H-4′, H-5′ and H-1′); 7.98 (d, J = 8.1 Hz, 1H, H-8′); 7.69 (dd, J = 8.9 Hz and 1.8 Hz,1H, H-3′); 7.58 (~t, J ~8 Hz, 1H, H-7′); 7.55 (~t, J ~8 Hz, 1H, H-6′); 6.11 (s, 1H, H-4); 2.38 (s, 3H, C$\underline{H}_3$ on C-3); 2.22 (s, 3H, C$\underline{H}_3$ on C-5). ^{13}C-NMR (DMSO-d_6): 148.6 (C-3); 139.9 (C-5); 137.6 (C-2′); 133.4 (C-8′a); 131.9 (C-4′a); 129.3 (C-4′); 128.5 (C5′); 128.1 (C-8′); 127.3 (C-7′); 126.7 (C-6′); 123.4 (C-3′); 121.9 (C-1′); 107.8 (C-4); 13.8 (C$\underline{H}_3$ on C-5); 12.8 (C$\underline{H}_3$ on C-3). Anal. calcd. for $C_{15}H_{14}N_2$: C, 81.05%; H, 6.35%; N, 12.60%. Found: C, 81.68%; H, 6.49%; N, 12.48%.

4.4.14. 1-(4-Methoxyphenyl)-3,5-dimethyl-1H-pyrazole (**8d**)

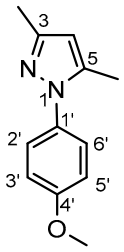

Thick yellow oil. ^{1}H-NMR (CDCl$_3$): 7.32 (d, J = 8.5 Hz, 2H, H-2′,6′); 6.95 (d, J = 8.5 Hz, 2H, H-3′,5′); 5.97 (s, 1H, H-4); 3.83 (s, 3H, OC$\underline{H}_3$); 2.29 (s, 3H, C$\underline{H}_3$ on C-3); 2.24 (s, 3H, C$\underline{H}_3$ on C-5). ^{13}C-NMR (CDCl$_3$): 158.8 (C-4′); 148.4 (C-3); 139.6 (C-5); 132.9 (C-1′); 126.4 (C-2′,6′); 114.1 (C-3′,5′); 106.7 (C-4); 55.5 (O$\underline{C}$H$_3$); 13.4 (C$\underline{H}_3$ on C-5); 12.1 (C$\underline{H}_3$ on C-3). Anal. calcd. for $C_{12}H_{14}N_2O$: C, 71.26%; H, 6.98%; N, 13.85%. Found: C, 71.59%; H, 7.03%; N, 13.71%

4.4.15. 8′-(3,5-dimethyl-1H-pyrazol-1-yl)-4,5′-bis(methylthio)-1′-(naphthalen-2-yl)-1′H- 1,2′-bipyridazino[4,5-d]pyridazine (**32c**)

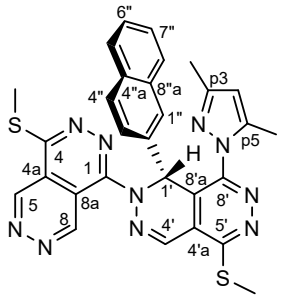

Yellowish powder. M.p. 245-247 °C. ^{1}H-NMR (CDCl$_3$): 10.53 (d, J = 1.1 Hz, 1H, H-8); 9.72 (d, J=1.1 Hz, 1H, H-5); 8.064 and 8.059 (2xs, 2H, H-4′ and H-1′, resp.); 7.62 (m, 1H, H-5″); 7.55 (d, J = 8.6 Hz, 1H, H-4″); 7.53 (m, 1H, H-8″); 7.35-7.30 (m. 2H, H-6″ and H-7″); 7.18 (br s, 1H, H-1″); 6.91 (dd, J = 8.6 Hz and 1.6 Hz, 1H, H-3″); 6.07 (s, 1H, H-p4); 2.77 (s, 3H, SC$\underline{H}_3$ on C-5′); 2.70 (s, 3H, SC$\underline{H}_3$ on C-4); 2.35 (s, 3H, C$\underline{H}_3$ on C-p5); 2.04 (s, 3H, C$\underline{H}_3$ on C-p3). ^{13}C-NMR (CDCl$_3$): 156.7 (C-5′); 155.4 (C-4); 152.5 (C-p3); 150.7 (C-8′), 149.7 (C-1); 148.8 (C-8); 146.4 (C-5); 142.8 (C-p5); 136.4 (C-2″); 133.4 (two coalesced lines, C-4′ and C-4″a); 133.3 (C-8″a); 129.2 (C-4″); 128.8 (C-5″); 128.4 (C-7″); 127.9 (C-8″); 126.87 (C-6″); 126.83 (C-4′a); 125.4 (C-1″); 123.9 (C-3″); 120.5 (two coalesced lines, C-4a and C-8′a); 113.1 (C-8a); 108.7 (C-p4); 53.8 (C-1′); 13.7 (SC$\underline{H}_3$ on C-5′); 13.5 (SC$\underline{H}_3$ on C-4); 14.4 (C$\underline{H}_3$ on C-p5); 12.3 (C$\underline{H}_3$ on C-

 doi:10.20944/preprints202506.1204.v1

p3). Anal. calcd. for $C_{29}H_{24}N_{10}S_2$: C, 60.40%; H, 4.19%; N, 24.29%; S, 11.12%. Found: C, 60.62%; H, 4.27%; N, 24.20%; S, 11.03%.

4.4.16. 1-butoxy-4-(methylthio)pyridazino[4,5-d]pyridazine (**33**)

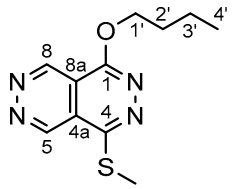

Light yellow powder. M.p. 96-99 °C. ^{1}H-NMR ($CDCl_3$): 9.89 (d, *J* = 1.2 Hz, 1H, H-8); 9.88 (d, *J* = 1.2 Hz, 1H, H-5); 4.71 (t, *J* = 6.7 Hz, 2H, H-1′); 2.84 (s, 3H, SC<u>H</u>$_3$ on C-4); 1.95 (~qi, *J* ~ 7 Hz, 2H, H-2′); 1.58 (~sex, , *J* ~ 7 Hz, 2H, H-3′); 1.03 (t, *J* = 7.4 Hz, 3H, H-4′). ^{13}C-NMR ($CDCl_3$): 158.2 (C-1); 154.1 (C-4); 146.3 (C-8); 146.1 (C-5); 120.7 (C-4a); 112.6 (C-8a); 68.9 (C-1′); 31.1 (C-2′); 19.6 (C-3′); 14.2 (C-4′); 13.3 (S<u>C</u>H$_3$ on C-4). Anal. calcd. for $C_{11}H_{14}N_4OS$: C, 52.78%; H, 5.64%; N, 22.38%; S, 12.81%. Found: C, 52.99%; H, 5.69%; N, 22.45%; S, 12.91%.

4.4.17. 4,5′,8′-tris(methylthio)-1′-(naphthalen-2-yl)-1′H-1,2′-bipyridazino[4,5-d]pyridazine (**34c**)

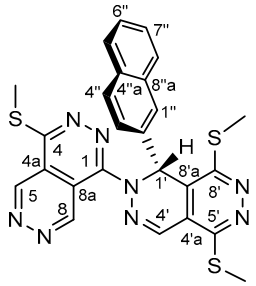

Light yellowish powder. M.p. 214-216 °C. ^{1}H-NMR ($CDCl_3$): 10.57 (d, *J* = 1.1 Hz, 1H, H-8); 9.72 (d, *J*=1.1 Hz, 1H, H-5); 8.05 (s, 1H, H-4′); 7.81 (br s, 1H. H-1″); 7.71-7.64 and 7.65 (overlapping m's and br s, 4H, H-4″, H-5″, H-8″ and H-1′, resp.); 7.61 (dd, *J* = 8.6 Hz and 1.8 Hz, 1H, H-3″); 7.37-7.34 (m, 2H, H-6″ and H-7″); 2.78 (s, 3H, SC<u>H</u>$_3$ on C-4); 2.76 (s, 3H, SC<u>H</u>$_3$ on C-5′); 2.66 (s, 3H, SC<u>H</u>$_3$ on C-8′). ^{13}C-NMR ($CDCl_3$): 156.8 (C-8′); 155.3 (C-4); 153.6 (C-5′); 150.7 (C-8′), 149.6 (C-1); 148.9 (C-8); 146.4 (C-5); 134.7 (C-2″); 134.6 (C-4′); 133.7 (C-4″a);133.2 (C-8″a); 129.2 (C-4″); 128.8 (C-8″); 128.3 (C-1″); 127.2 (C-7″); 126.9 (C-6″); 126.4 (C-4′a); 125.9 (C-3″); 120.6 (C-4a); 117.8 (C-8′a);113.0 (C-8a); 53.6 (C-1′); 14.1 (S<u>C</u>H$_3$ on C-8′); 13.58 (S<u>C</u>H$_3$ on C-4); 13.54 (S<u>C</u>H$_3$ on C-5′). ^{15}N-NMR chemical shifts [ref.: d(NH_3) = 0 ppm] detectable by ^{1}H-^{15}N-HMBC ($CDCl_3$): 396 (not resolved, N-6 and N-7 as identified *via* cross-peaks with H-5 and H-8 signals); 335 (N-3′, as identified *via* cross-peak with H-1′ signal); 155 (N-2′, as identified *via* cross-peak with H-1′ signal). Anal. calcd. for $C_{25}H_{20}N_8S_3$: C, 56.80%; H, 3.81%; N, 21.20%; S, 18.19%. Found: C, 56.67%; H, 3.92%; N, 21.25%; S, 18.11%.

4.4.18. 1,4-Bis(methylthio)pyridazino[4,5-d]pyridazine (**I**)

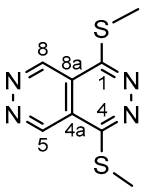

 doi:10.20944/preprints202506.1204.v1

Yellow powder. M.p. 190-193 °C. ^{1}H-NMR ($CDCl_3$): 9.76 (s, 2H, H-5,8); 2.86 (s, 6H, SC$\underline{H}_3$ on C-1 and C-4). Anal. calcd. for $C_8H_8N_4S_2$: C, 42.84%; H, 3.60%; N, 24.98%; S, 28.59%. Found: C, 43.02%; H, 3.72%; N, 24.85%; S, 28.67%.

4.4.19. 1-(3,5-Dimethyl-1H-pyrazol-1-yl)-4-(methylthio)pyridazino[4,5-d]pyridazine (**II**)

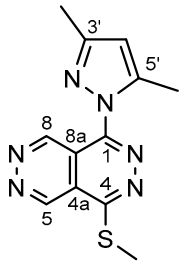

Yellow powder. M.p. 223-226 °C. ^{1}H-NMR ($CDCl_3$): 10.44 (d, J = 1.2 Hz, 1H, H-8); 9.86 (d, J = 1.2 Hz, 1H, H-5); 6.17 (s, 1H, H-4′); 2.91 (s, 3H, SC$\underline{H}_3$); 2.62 (s, 3H, C$\underline{H}_3$ on C-5′); 2.36 (s, 3H, C$\underline{H}_3$ on C-3′). Anal. calcd. for $C_{12}H_{12}N_6S$: C, 52.93%; H, 4.44%; N, 30.86%; S, 11.17%. Found: C, 53.06%; H, 4.32%; N, 30.65%; S, 11.22%.

5. Conclusions

This contribution presents an in-depth synthetic and mechanistic study on the complex and intriguing transformations of 1,2,4a,8a-tetrahydro-1-arylpyridazino[4,5-*d*] pyridazines **1a–e** and **2a–e**. Besides the expected aromatic heterocycles **3a–e** the DDQ-mediated reactions catalyzed by ferrocene afforded a variety of unexpected products. The research disclosed novel types of heterocyclic transformations controlled by the substitution pattern of the substrate molecules. The proposed mechanisms were analyzed and confirmed by theoretical modelling of the key elementary steps which initiate the competing pathways leading to the formation of the different types of products. The newly recognized transformations along with the specific structure-reactivity correlations reported in this contribution might also be utilized in other fields of modelling-supported synthetic chemistry.

Supplementary Materials: The following are available online at Preprints.org, **S1**: Copies of the 1D- and 2D-NMR spectra.

Author Contributions: For research articles with several authors, a short paragraph specifying their individual contributions must be provided. The following statements should be used “Conceptualization, A.Cs., and D.H..; methodology, D.H., V.E. and A.Cs.; software, A.Cs. and T.Zs.N.; validation, D.H.; formal analysis, V.E. and T.Zs.N; investigation, D.H.; V.E. T.Zs.N. and A.Cs.; resources, A.Cs.; data curation, T.Zs.N. writing—original draft preparation, D.H. and A.Cs.; writing—review and editing, A.Cs.; visualization, A.Cs.; supervision, V.E.; project administration, D.H.; funding acquisition, A.Cs. All authors have read and agreed to the published version of the manuscript.

Funding: This research was financially supported by the Hungarian Scientific Research Fund [OTKA K_129037], Hungary and by the ELTE Thematic Excellence Program supported by the Hungarian Ministry for Innovation and Technology. [SzintPlusz_1117].

Institutional Review Board Statement: Not applicable.

Informed Consent Statement: Not applicable.

Data Availability Statement: The data generated and analyzed during our research are not available in any public database or repository but will be shared by the corresponding author upon reasonable request.

 doi:10.20944/preprints202506.1204.v1

Acknowledgments: Authors express their gratitude to Mr. Antonio Dembo for his valuable help in the experimental work.

Conflicts of Interest: The authors declare no conflict of interest.

References

1. Akahane, A.; Katayama, H.; Mitsunaga, T.; Kato, T.; Kinoshita, T.; Kita, Y.; Kusunoki, T.; Terai, T.; Yoshida, K.; Shiokawa, Y. Discovery of 6-Oxo-3-(2-phenylpyrazolo[1,5-a]pyridin-3-yl)-1(6H)-pyridazinebutanoic Acid (FK 838): A Novel Non-Xanthine Adenosine A1 Receptor Antagonist with Potent Diuretic Activity. *J. Med. Chem*. **1999**, *42*, 779–783.
2. Meade, E.A.; Wotring, L.L.; Drach, J.C.; Townsend, L.B. Synthesis and Antiproliferative and Antiviral Activity of Carbohydrate Modified Pyrrolo[2,3-d]pyridazin-7-one Nucleosides. *J. Med. Chem*. **1997**, *40*, 794–801.
3. Kimura, T.; Fujihara, Y.; Shibakawa, N.; Fujiwara, H.; Itoh, E.; Matsunobu, K.; Tabata, K.; Yasuda, H. Pyrrolopyridazine Derivatives. U.S. Patent 6063782 A, 17 July 1996. 18. Siddiqui, A.A.; Mishra, R.; Shaharyar, M. Synthesis, characterization and antihypertensive activity of pyridazinone derivatives. *Eur. J. Med. Chem*. **2010**, *45*, 2283–2290.
4. Siddiqui, A.A.; Mishra, R.; Shaharyar, M. Synthesis, characterization and antihypertensive activity of pyridazinone derivatives. *Eur. J. Med. Chem*. **2010**, *45*, 2283–2290. https://doi.org/10.1016/j.ejmech.2010.02.003.
5. Refaat, H.M.; Khalil, O.M.; Kadry, H.H. Synthesis and anti-inflammatory activity of certain piperazinylthienylpyridazine derivatives. *Arch. Pharm. Res*. **2007**, *30*, 803–811.
6. Malinka, W.; Redzicka, A.; Lozach, O. New derivatives of pyrrolo [3,4-d]pyridazinone and their anticancer effects. *Farmaco* **2004**, *59*, 457–462.
7. Jiang, J.; Boxer, M.B.; van der Heiden, M.G.; Shen, M.; Skoumbourdis, A.P.; Southall, N.; Veith, H.; Leister, W.; Austin, C.P.; Park, H.W.; et al. Evaluation of thieno [3,2-b]pyrrole [3,2-d]pyridazinones as activators of the tumor cell specific M2 isoform of pyruvate kinase. *Bioorg. Med. Chem. Lett*. **2010**, *20*, 3387–3393.
8. Abd El-Ghaffar, N.F.; Mohamed, M.K.; Kadah, M.S.; Radwan, A.M.; Said, G.H.; Abd Al, S.N. Synthesis and antitumor activities of some new pyridazinones containing the 2-phenyl-1H-indolyl moiety. *J. Chem. Pharm. Res*. 2011, *3*, 248–259.
9. Rathish, I.; Javed, K.; Ahmad, S.; Bano, S.; Alam, M.; Akhter, M.; Pillai, K.; Ovais, S.; Samim, M. Synthesis and evaluation of anticancer activity of some novel 6-aryl-2-(p-sulfamylphenyl)-pyridazin-3(2H)-ones. *Eur. J. Med. Chem*. **2012**, *49*, 304–309.
10. Gutierrez, D.A.; DeJesus, R.E.; Contreras, L.; Rodriguez-Palomares, I.A.; Villanueva, P.J.; Balderrama, K.S.; Monterroza, L.; Larragoity, M.; Varela-Ramirez, A.; Aguilera, R.J. A new pyridazinone exhibits potent cytotoxicity on human cancer cells via apoptosis and poly-ubiquitinated protein accumulation. *Cell Biol. Toxicol*. **2019**, *35*, 503–519.
11. Sabelli, C.; Tangocci, P.; Zanazzi, P. F. The crystal structure of pyridazino[4,5-d]pyridazine, *Acta Cryst*. **1969**, B25, *11*, 2231–2236.
12. Zhylenko, I.S.; Solntsev, P.V.; Rusanov, E.B.; Chernega, A.N.; Domasevitch, K.V. Hydrate frameworks involving the pyridazino[4,5-d]pyridazine unit as a multiple hydrogen-bond acceptor. *Acta Crystallogr C*. **2008**, *64*, 237–241. doi:10.1107/S0108270108007117.
13. Haider, N. Inverse-electron-demand Diels-Alder reactions of condensed pyridazines, part 1. Synthesis of phthalazine derivatives from pyridazino[4,5-*d*]pyridazines. *Tetrahedron*, **1991**, *47*, 3959–3968. doi.: 10.1016/S0040-4020(01)86436-X.
14. Heinisch, G.;. Kirchner, I. *Monatsh. Chem*. **1979**, *210*, 365.
15. Heinisch, G.; Jentzsch, A.; Pailer, M. *Monatsh. Chem*. **1974**, *205*, 648.
16. Braun, M.; Hanel, G.; Heinisch, G. *Monatsh. Chem*. **1978**, *109*, 63.
17. Haider, N.; Heinisch, G.; Kirchner, I. Pyridazin-Analoga biologisch aktiver Verbindungen, 2. Mitt. 4-Aryl-pyridazino[4,5-d]pyridazine mit cyclischem Amin-Substituenten an C-1. Arch. Pharm., **1982**, *315*, 778–773. doi: 10.1002/ardp.19823150909.

 doi:10.20944/preprints202506.1204.v1

18. Nagy, Zs.T.; Lőrincz, K.; Csámpai, A.; Kotschy, A. The selective functionalization of pyridazino[4,5-*d*]pyridazines using polar organometallic reagents. *Heterocycles*, **2007**, *71*, 141–151.
19. Csámpai, A.; Abrán, Á.; Kudar, V.; Túrós, Gy.; Wamhoff, H.; Sohár, P. Synthesis, NMR, IR spectroscopic and X-ray study of novel [pyridazin-3(2H)-one-6-yl]ferrocenes and related ferrocenophane derivatives. Study on ferrocenes. Part 14. *J. Organomet. Chem*., **2005**, *690*, 802–810. doi: 10.1016/j.jorganchem.2004.09.086.
20. Csókás, D.; Zupkó, I.; Károlyi, B.I.; Drahos, L.; Holczbauer, T.; Palló, A.; Czugler, M.; Csámpai, A. Synthesis, spectroscopy, X-ray analysis and in vitro antiproliferative effect of ferrocenylmethylene-hydrazinylpyridazin-3(2H)-ones and related ferroceno[d]pyridazin-1(2H)-ones. *J. Organomet. Chem*., **2013**, *743*, 130-138. https://doi.org/ 10.1016/j.jorganchem.2013.06.040.
21. Csókás, D.; Károlyi, B.I.; Bősze, Sz.; Szabó, I.; Báti, G.; Drahos, L.; Csámpai, A. 2, 3-Dihydroimidazo[1,2-b]ferroceno[d]pyridazines and a 3,4-dihydro-2H-pyrimido[1,2-b]ferroceno[d]pyridazine: Synthesis, structure and in vitro antiproliferation activity on selected human cancer cell lines. *J. Organomet. Chem*., **2014**, *750*, 41-48. https://doi.org/10.1016/j.jorganchem.2013.10.057.
22. Jernei, T.; Bősze, Sz.; Szabó, R.; Hudecz, F.; Majrik, K.; Csámpai, A. N-ferrocenylpyridazinones and new organic analogues: Synthesis, cyclic voltammetry, DFT analysis and in vitro antiproliferative activity associated with ROS-generation. *Tetrahedron*, **2017**, *73*, 6181-6192. https://doi.org/10.1016/j.tet.2017.09.015.
23. Alaoui, N.-E.E.; Boulhaoua, M.; Hutai, D.; Oláh-Szabó, R.; Bősze, S.; Hudecz, F.; Csámpai, A. Synthetic and DFT Modelling Studies on Suzuki–Miyaura Reactions of 4,5-Dibromo-2-methylpyridazin-3(2*H*)-one with Ferrocene Boronates, Accompanied by Hydrodebromination and a Novel Bridge-Forming Annulation In Vitro Cytotoxic Activity of the Ferrocenyl–Pyridazinone Products. *Catalysts*, **2022**, *12*, 578. https://doi.org/10.3390/catal12060578.
24. Hati, S.; Holzgrabe, U.; Sen, S. Oxidative dehydrogenation of C–C and C–N bonds: A convenient approach to access diverse (dihydro)heteroaromatic compounds. *Beilstein J. Org. Chem*. **2017**, *13*, 1670–1692. https://doi.org./10.3762/bjoc.13.162.
25. Gaikwad, S.; Kovacikova, L.; Pawar, P.; Gaikwad, M.; Bohác, A.; Dawane, B. An updates: Oxidative aromatization of THβC to β-carbolines and their application for the β-carboline alkaloids synthesis. *Tetrahedron*, **2024**, *155*, 133903. https://doi.org/10.1016/j.tet.2024.133903.
26. Fatykhov, R.F.; Khalymbadzha, I.A.; Sharapov, A.D.; Potapova, A.P.; Mochulskaya, N.N.; Tsmokalyuk, A.N.; Ivoilova, A.V.; Mozharovskaia, P.N.; Santra, S.; Chupakhin, O.N. MnO_2-Mediated Oxidative Cyclization of "Formal" Schiff's Bases: Easy Access to Diverse Naphthofuro-Annulated Triazines. *Molecules* **2022**, *27*, 7105. https://doi.org/10.3390/molecules27207105.
27. Utecht-Jarzyńska, G.; Kowalczyk, A.; Jasiński, M. Fluorinated and Non-Fluorinated 1,4-Diarylpyrazoles via MnO_2-Mediated Mechanochemical Deacylative Oxidation of 5-Acylpyrazolines. *Molecules* **2022**, *27*, 8446. https://doi.org/10.3390/molecules27238446.
28. Yadav, J. S.; Reddy, B. V. S.; Basak, A. K.; Baishya, G.; Narsaiah, A. V. Iodoxybenzoic acid (IBX): An efficient and novel oxidizing agent for the aromatization of 1,4-dihydropyridines. *Synthesis* **2006**, 451–454. https://doi.org/ 10.1055/s-2005-918519.
29. Nageswar, Y.V.D.; Ramesh, K., Rakhi, K. IBX-Mediated Organic Transformations in Heterocyclic Chemistry-A Decade Update. *Frontiers in Chemistry*, **2022**, *10*, 841751. https://doi.org/10.3389/fchem.2022.841751.
30. Varala, R.; Seema, V.; Alam, M.M.; Dubasi, N.; Vummadi, R.D. Iodoxybenzoic Acid (IBX) in Organic Synthesis: A Septennial Review**.** *Curr. Org. Synth***.,** **2024**, *21*, 607–664. https:/doi.org/ 10.2174/0115701794263252230924074035.
31. Hati, S.; Sen, S. *Tetrahedron Lett*. **2016**, *57*, 1040–1043. doi:10.1016/j.tetlet.2016.01.081
32. Yang, R.; Xiong, Y.; Deng, S.; Bai, J.; Song, X.-R.; Xiao, Q. NBS-mediated bromination and dehydrogenation of tetrahydro-quinoline in one pot: scope and mechanistic study. *RSC Adv*., **2023**, *13*, 33495–33499. https://doi.org/10.1039/D3RA06747E**.**
33. Kamal, A.; Sathish, M.; Prasanthi, A.V.G.; Chetna, J.; Tangella, Y.; Srinivasulu, V.; Shankaraiah, N.; Alarifi, A., An efficient one-pot decarboxylative aromatization of tetrahydro-β-carbolines by using *N*-chlorosuccinimide: total synthesis of norharmane, harmane and eudistomins. *RSC. Adv*., **2015**, *5*, 90121-90126. https://doi.org/10.1039/C5RA16221A**.**

 doi:10.20944/preprints202506.1204.v1

34. Zhao, D.; Wang, T.; Li, J.-X. *Chem. Commun*. **2014**, *50*, 6471–6474. doi:10.1039/C4CC02648A
35. Litvić, M.; Cepanec, I.; Filipan, M.; Kos, K.; Bartolinčić, A.; Družković, V.; Tibi, M.M.; Vinković, V., Mild, selective, and high-yield oxidation of hantzsch 1,4-dihydropyridines with lead(IV) acetate, *Heterocycles*, **2005**, *65*, 23–35. https://doi.org/ 10.3987/COM-04-10194.
36. Hussain, K.; Wadhwa, D., Highly Efficient, One Pot Synthesis and Oxidation of Hantsch 1,4-Dihydropyridines Mediated by Iodobenzene Diacetate (III) Using Conventional Heating, Ultrasonic and Microwave Irradiation. *Int. J. Org. Chem*., **2014**, *4*, 174–181. https://doi.org/ 10.4236/ijoc.2014.43019.
37. Varma, R. S.; Kumar, D. J. Solid state oxidation of 1,4-dihydropyridines to pyridines using phenyliodine(III) bis(trifluoroacetate) or elemental sulfur. *Chem. Soc., Perkin Trans. 1* **1999**, 1755–1757. https://doi.org/10.1039/A809494B.
38. Szabó, T.; Hazai, V.; Volk, B.; Milen, M. Simig, Gy. First total synthesis of the β-carboline alkaloids trigonostemine A, trigonostemine B and a new synthesis of pityriacitrin and hyrtiosulawesine. *Tetrahedron Lett*., **2019**, *60*, 1471–1475. https://doi.org/10.1016/j.tetlet.2019.04.044.
39. Manasa, K.L.; Tangella, Y.; Ramu, G.; Babu, B.N. TCCA; A Mild Reagent for Decarboxylative/Dehydrogenative Aromatization of Tetrahydro-β-carbolines: Utility in the Total Synthesis of Norharmane, Harmane, Eudistomin U, I and N. *ChemistrySelect*, **2017**, *2*, 9162–9167. https://doi.org/10.1002/slct.201701886.
40. Zeynizadeh, B.; Dilmaghani, K.A.; Roozijoy, A., Aromatization of Hantzsch Ester 1,4-Dihydropyridines with Iodine under Normal Conditions and Ultrasound Irradiation. *J. Chin. Chem. Soc*., **2005**, *52*, 1001–1004. https://doi.org/10.1002/jccs.200500139.
41. Liu, Y.; Hu, H.; Wang, X.; Zhi, S.; Kan, Y.; Wang, C., Synthesis of Pyrrole via a Silver-Catalyzed 1,3-Dipolar Cycloaddition/Oxidative Dehydrogenative Aromatization Tandem Reaction. J. Org. Chem. 2017, 82, 8, 4194–4202. https://doi.org/10.1021/acs.joc.7b00180.
42. Kumar, P.; Kadyan, K.; Duhan, M.; Sindhu, J.; Hussain, K.; Lal, S. Silica-supported ceric ammonium nitrate (CAN): a simple, mild and solid-supported reagent for quickest oxidative aromatization of Hantzsch 1,4-dihydropyridines. *Chem. Pap.* **2019**, *73*, 1153–1162. https://doi.org/10.1007/s11696-018-0666-5.
43. Zolfigol, M.A.; Salehi, P.; Ghorbani-Choghamarani, A.; Safaiee, M.; Shahamirian, M., Silica Chromate as a Novel Oxidizing Agent for the Oxidation of 1,4-Dihydropyridines, *Synth. Commun*, **2007**, *37*, 1817–1823. https://doi.org/10.1080/00397910701316276.
44. Cai, X.-H.; Yang, H.-J.; Guo-lin Zhang, G.-L., Aromatization of 1,4-dihydropyridines with selenium dioxide *Can. J. Chem*. **2005**, *83*: 273–275. https://doi.org/ 10.1139/V05-058**.**
45. Zhu, X.-Q.; Zhao, B.-J.; Cheng, J.-P. Mechanisms of the Oxidations of NAD(P)H Model Hantzsch 1,4-Dihydropyridines by Nitric Oxide and Its Donor *N*-Methyl-N-nitrosotoluene-p-sulfonamide. *J. Org. Chem*., **2000**, *65*, 8158–8163. https://doi.org/10.1021/jo000484h.
46. Li, X.; Li, C.; Yin, B.; Li, C.; Liu, P.; Li, J.; Shi, Z., DDQ-Induced Dehydrogenation of Heterocycles for CC Double Bond Formation: Synthesis of 2-Thiazoles and 2-Oxazoles. *Chem. Asian J*. **2013**, *8*, 1408–14011. https://doi.org/10.1002/asia.201300267.
47. Patir, S.; Ertürk, E., An Entry to the Azocino[4,3-b]indole Framework through a Dehydrogenative Activation of 1,2,3,4-Tetrahydrocarbazoles Mediated by DDQ: Formal Synthesis of (±)-Uleine. *J. Org. Chem*. **2011**, *76*, 335–338. https://doi.org/10.1021/jo1021663.
48. Alsharif, M.A.; Raja, Q.A.; Majeed, N.A.; Jassas, R.S.; Alsimaree, A.A.; Sadiq, A.; Naeem, N.; Mughal, E.U.; Alsantali, R.I.; Moussa, Z.; Ahmed, S.A. DDQ as a versatile and easily recyclable oxidant: a systematic review. *RSC Adv*., **2021**, *11*, 29826–29858. https://doi. 10.1039/D1RA04575J.
49. Bisek, B.; Chaladaj, W. Access to 2-Alkenyl-furans via a Cascade of Pd-Catalyzed Cyclization/Coupling Followed by Oxidative Aromatization with DDQ. *J. Org. Chem*. **2024**, *89*, *10*, 7275–7279. https://doi.org/10.1021/acs.joc.4c00149.
50. Knall, A.-C.; M. Hollauf, M.; Slugovc, C. Kinetic studies of inverse electron demand Diels–Alder reactions (iEDDA) of norbornenes and 3,6-dipyridin-2-yl-1,2,4,5-tetrazine. *Tetrahedron Lett*., **2014**, *55*, 4763–4766. https://doi.org/10.1016/j.tetlet.2014.07.002.
51. Zjang, J.; Zhang, H.; Wang, Z.; Yao, W. Concise Synthesis of Tetrasubstituted 1,6-Dihydropyridazine and Pyridazine Derivatives. *Synthesis*, **2024**; *56*, 3915–3922. https://doi.org/10.1055/a-2445-1338.

 doi:10.20944/preprints202506.1204.v1

52. Litvic', M.F.; Litvic, M.; Vinkovic, V. An efficient, metal-free, room temperature aromatization of Hantzsch 1,4-dihydropyridines with urea–hydrogen peroxide adduct, catalyzed by molecular iodine, *Tetrahedron*, **2008**, *64*, 5649–5656. https://doi.org/10.1016/j.tet.2008.04.040.
53. Tuo, X.; Chen, S.; Jiang, P.; Ni, P.; Wang, X.; Deng, G-J. Iodine-catalyzed convergent aerobic dehydroaromatization toward benzazoles and benzazines. *RSC Adv.*, **2020**, *10*, 8348–8351. https://doi.org/10.1039/c9ra10964a.
54. Hati, S.; Sen, S. Cerium Chloride Catalyzed, 2-Iodoxybenzoic Acid Mediated Oxidative Dehydrogenation of Multiple Heterocycles at Room Temperature. *Eur. J. Org. Chem.*, **2017**, *3*, 1277–1280 https://doi.org/10.1002/ejoc.201601419.
55. Zhou, W.; Taboonpong, P.; Aboo, A.H.; Zhang, L.; Jiang, J.; Xiao, J. A Convenient Procedure for the Oxidative Dehydrogenation of N-Heterocycles Catalyzed by $FeCl_2$/DMSO. *Synlett*, **2016**, *27*, 1806–1809. https://doi.org/10.1055/s-0035-1561613
56. Jung, D.; Kim, M.H.; Kim, J. Cu-Catalyzed Aerobic Oxidation of Di-*tert*-butyl Hydrazodicarboxylate to Di-*tert*-butyl Azodicarboxylate and Its Application on Dehydrogenation of 1,2,3,4-Tetrahydroquinolines under Mild Conditions. *Org. Lett*. **2016**, *18*, 6300–6303. https://doi.org/10.1021/acs.orglett.6b03166.
57. Iosub, A. V.; Stahl, S. S. Catalytic Aerobic Dehydrogenation of Nitrogen Heterocycles Using Heterogeneous Cobalt Oxide Supported on Nitrogen-Doped Carbon**.** *Org. Lett*. **2015**, *17*, 4404–4407. https://doi.org/10.1021/acs.orglett.5b01790.
58. Fujita, K.; Tanaka, Y.; Kobayashi, M.; Yamaguchi, R. Homogeneous perdehydrogenation and perhydrogenation of fused bicyclic N-heterocycles catalyzed by iridium complexes bearing a functional bipyridonate ligand. *J. Am. Chem. Soc*. **2014**, *136*, 4829–4832. https://doi.org/10.1021/ja5001888.
59. Wu, J.; Talwar, D.; Johnston, S.; Yan, M.; Xiao, J. Acceptorless dehydrogenation of nitrogen heterocycles with a versatile iridium catalyst. *Angew. Chem., Int. Ed*. **2013**, *52*, 6983–6987. https://doi.org/10.1002/anie.201300292.
60. Sun, X.; Zhu, J.; Xia, Y.; Wu, L. Palladium Nanoparticles Stabilized by Metal–Carbon Covalent Bonds as an Expeditious Catalyst for the Oxidative Dehydrogenation of Nitrogen Heterocycles. *ChemCatChem,* **2017**, *9*, 2463–2466. https://doi.org/10.1002/cctc.201700370.
61. *Jawale, D.V.; Gravel, E.; Shah, N.; Dauvois, V.; Li, H.; Namboothiri, I.N.; Doris, E. Cooperative dehydrogenation of* N-heterocycles using a carbon nanotube-rhodium nanohybrid. *Chemistry*. **2015**, *21*, 7039–7042. https://doi.org/10.1002/chem.201500148.
62. Wu, Y.; Chen, Z.; Cheong, W. C.; Zhang, C.; Zheng, L.; Yan, W.; Yu, R.; Chen, C.; Li, Y. Nitrogen-coordinated cobalt nanocrystals for oxidative dehydrogenation and hydrogenation of N-heterocycles. *Chem. Sci*. **2019**, *10*, 5345–5352. https://doi.org/10.1039/C9SC00475K.
63. Hu, Y.; Li, X.; Liu, M.; Bartling, S.; Lund, H.; Rabeah, J.; Dyson, P.J.; Beller, M.; Jagadeesh, R.V. A Cobalt Nanocatalyst for the Hydrogenation and Oxidative Dehydrogenation of *N*-heterocycles. *ChemCatChem*. **2024**, *16*, e202301027. https://doi.org/10.1002/cctc.202301027.
64. Sun. K.; Shan, H.; Ma, R.; Wang, P.; Neumann, H.; Lu, G.-P.; Beller, M. Catalytic oxidative dehydrogenation of *N*-heterocycles with nitrogen/phosphorus co-doped porous carbon materials. Chem. Science, 2022, 13, 6865–6872. https://doi.org/10.1039/D2SC01838A.
65. Girard, S.A.; Huang, H.; Zhou, F.; Deng, G.-J.; Li, C.-J. Catalytic dehydrogenative aromatization: an alternative route to functionalized arenes. *Org. Chem. Front*. **2015**, *2*, 279–287. https://doi.org/10.1039/C4QO00358F.
66. Kirsch, S.F.; Wegener, M. Oxidation by dehydrogenation. *Comprehensive Org. Synth. II.* **2014**, *7*, 1–25. 10.1016/B978-0-08-097742-3.00701-1
67. Zhang, T.; Lv. Y.; Zhang, Z.; Jia, Z.; Loh, T.-P. A Rare Earth Metal Catalyzed Aerobic Dehydrogenation of N-Heterocycles. *Org. Lett*., **2023**, *25*, 4468–4472. https://doi.org/10.1021/acs.orglett.3c01449.
68. Nakamichi, N.; Kawashita, Y.; Hayashi M. Oxidative aromatization of 1,3,5-trisubstituted pyrazolines and Hantzsch 1,4-dihydropyridines by Pd/C in acetic acid. *Org Lett*. **2002** *4*, 3955–3957 https://doi.org/10.1021/ol0268135
69. Bera, S.; Bera, A.; Banerjee, D., Nickel-Catalyzed Dehydrogenation of N-Heterocycles Using Molecular Oxygen. *Org. Lett.* **2020**, *22*, 6458–6463. https://doi.org/10.1021/acs.orglett.0c02271.

 doi:10.20944/preprints202506.1204.v1

70. Jia, Z., Yang, Q.; Zhang, L.; Luo, S. Photoredox Mediated Acceptorless Dehydrogenative Coupling of Saturated N-Heterocycles. *ACS Catal.* **2019**, *9*, 3589–3594. https://doi.org/10.1021/acscatal.9b00123.
71. Wang, Z.; Zhao, R.; Li, W.; Sun, H.; Chen, G.; Zhan, F.; Zhao, H. Enhanced catalytic performance for aerobic dehydrogenation of *N*-heterocycles over bimetallic CoO_x-CeO_2 catalysts derived from Ce-based MOFs. *Molecular Catalysis*, **2024**, *567*, 114450. https://doi.org/10.1016/j.mcat.2024.114450.
72. Enders, L.; Casadio, D.S.; Aikonen, S.; Lenarda, A.; Wirtanen, T.; Hu, T.; Hitela, S.; Ribeiro, L.S.; Pereira, M. F. R.; Helaja, J. Air oxidized activated carbon catalyst for aerobic oxidative aromatizations of *N*-heterocycles. *Catal. Sci. Technol.*, **2021**, *11*, 5962–5972. https://doi.org/10.139/D1CY00878A.
73. Kobayashi, M.; Hikawa, H.; Enda, T.; Kikkawa, S.; Azumaya, I. Synthesis of 1-Aryl-β-Carbolines *via* a Pd-Catalyzed Oxidative Pictet-Spengler Reaction/Aromatization Cascade Using Benzylic Alcohols in Water. *Eur. J. Org. Chem*., **2025**, *28*, e202401269. https://doi.org/10.1002/ejoc.202401269.
74. Ju, S.; Zhou, X.; Jin, H.; Yang, Y.; Yang, L; Wu, J. Stereoselective oxidative C3–N bond dehydrogenation and aromatization of 1-carboxyl substituted tetrahydroisoquinolines employing pipecolate oxidase. *Green Synth. and Catal*., **2024**, in press https://doi.org/10.1016/j.gresc.2024.06.001.
75. Fabbrizzi, L. The ferrocenium/ferrocene couple: a versatile redox switch. *ChemTexts*, **2020**, *6*, 22 https://doi.org/10.1007/s40828-020-00119-6.
76. Chen, N.; Wu, Z.-J.; Xu, H.-C. Ferrocene as a Redox Catalyst for Organic Electrosynthesis. *Israel. J. Chem*., **2023**, *64*, e202300097. https://doi.org/10.1002/ijch.202300097.
77. Bauer, E.B. Recent Catalytic Applications of Ferrocene and Ferrocenium Cations in the Syntheses of Organic Compounds. *Molecules* **2024**, *29*, 5544. https://doi.org/10.3390/molecules29235544.
78. Astruc, D. The numerous paths of ferrocene. *Nat. Chem*. **2023**, *15*, 1650. https://doi.org/10.1038/s41557-023-01348-1.
79. Hernández-Muñoz, L.S.; Galano, A.; Astudillo-Sánchez, P.D.; Abu-Omar, M.M.; González, F.J. The mechanism of mediated oxidation of carboxylates with ferrocene as redox catalyst in absence of grafting effects. An experimental and theoretical approach. *Electrochim. Acta*, **2014**, *136*, 542–549, https://doi.org/10.1016/j.electacta.2014.04.189.
80. Sariga, V.A. The Renaissance of Ferrocene-Based Electrocatalysts: Properties, Synthesis Strategies, and Applications. *Top Curr Chem (Z)* **2023**, *381*, 32. https://doi.org/10.1007/s41061-023-00441-w.
81. Salman, H.M.A.; Mahmoud, M.R.; Abou-El-Wafa, M.H.M.; Rabie, U.M.; Crabtree, R.H. Redox reactions via outer sphere charge transfer complexation: the interaction of ferrocenes with σ- and -type acceptors. *Inorg. Chem. Commun*., **2004**, *7*, 1209–1212. https://doi.org/10.1016/j.inoche.2004.07.023.
82. Zhao, Y.; Truhlar, D.G. The M06 suite of density functionals for main group thermochemistry, thermochemical kinetics, noncovalent interactions, excited states, and transition elements: two new functionals and systematic testing of four M06-class functionals and 12 other functionals. *Theor. Chem. Account*, **2008**, *120*, 215–241. https://doi.org/10.1007/s00214-007-0310-x.
83. Hehre, J.W.; Radom, L.; Schleyer, P.V.R.; Pople, J.A. Ab initio molecular orbital theory, Wiley, New York, NY, USA, **1986**.
84. Tomasi, J.; Mennucci, B.; Cancès, E. The IEF version of the PCM solvation method: An overview of a new method addressed to study molecular solutes at the QM ab initio level. *J. Mol. Struct. THEOCHEM* **1999**, *464*, 211–226. https://doi.org/10.1016/S0166-1280(98)00553-3.
85. Alcarazo, M.; Kozhushkov, S.I. Synthetic Applications of Sulfonium Salts. *Eur. J. Inorg. Chem.* **2020**, *26*, 2486–2500. https://doi.org/10.1002/ejic.202000249.
86. Loco, D.; Chataigner, I.; Piquemal, J-P.; Spezia, R. Efficient and Accurate Description of Diels-Alder Reactions Using Density Functional Theory. *ChemPhysChem* **2022**, *23*, e202200349. http://doi.org/doi.org/10.1002/cphc.202200349.
87. Medina, J. M.; Mackey, J. L.; Garg, N. K.; Houk, K. N. The Role of Aryne Distortions, Steric Effects, and Charges in Regioselectivities of Aryne Reactions. *J. Am. Chem. Soc*. **2014**, *136*, 15798–15805. https://doi.org/10.1021/ja5099935.
88. Ricca, A.; Bauschlicher Jr., C.W.; Allamandola, L.J. The infrared spectroscopy of polycyclic aromatic hydrocarbons with five- and seven-membered fused ring defects. *The Astrophys. J*., **2011**, *729*, 94. https://doi.org/doi:10.1088/0004-637X/729/2/94.

 doi:10.20944/preprints202506.1204.v1

89. Gaussian 09, Revision A.02, M. J. Frisch, G. W. Trucks, H. B. Schlegel, G. E. Scuseria, M. A. Robb, J. R. Cheeseman, G. Scalmani, V. Barone, G. A. Petersson, H. Nakatsuji, X. Li, M. Caricato, A. Marenich, J. Bloino, B. G. Janesko, R. Gomperts, B. Mennucci, H. P. Hratchian, J. V. Ortiz, A. F. Izmaylov, J. L. Sonnenberg, D. Williams-Young, F. Ding, F. Lipparini, F. Egidi, J. Goings, B. Peng, A. Petrone, T. Henderson, D. Ranasinghe, V. G. Zakrzewski, J. Gao, N. Rega, G. Zheng, W. Liang, M. Hada, M. Ehara, K. Toyota, R. Fukuda, J. Hasegawa, M. Ishida, T. Nakajima, Y. Honda, O. Kitao, H. Nakai, T. Vreven, K. Throssell, J. A. Montgomery, Jr., J. E. Peralta, F. Ogliaro, M. Bearpark, J. J. Heyd, E. Brothers, K. N. Kudin, V. N. Staroverov, T. Keith, R. Kobayashi, J. Normand, K. Raghavachari, A. Rendell, J. C. Burant, S. S. Iyengar, J. Tomasi, M. Cossi, J. M. Millam, M. Klene, C. Adamo, R. Cammi, J. W. Ochterski, R. L. Martin, K. Morokuma, O. Farkas, J. B. Foresman, and D. J. Fox, Gaussian, Inc., Wallingford CT, 2016.